Cross-Talk between Myeloid-Derived Suppressor Cells and Mast Cells Mediates Tumor-Specific Immunosuppression in Prostate Cancer

Elena Jachetti[1], Valeria Cancila[2], Alice Rigoni[1], Lucia Bongiovanni[2], Barbara Cappetti[1], Beatrice Belmonte[2], Claudia Enriquez[1], Patrizia Casalini[3], Paola Ostano[5], Barbara Frossi[4], Sabina Sangaletti[1], Claudia Chiodoni[1], Giovanna Chiorino[5], Carlo E. Pucillo [4], Claudio Tripodo[2] and Mario P. Colombo[1].

[1] *Molecular Immunology Unit, Department of Research, Fondazione IRCCS Istituto Nazionale dei Tumori, Milan, Italy*

[2] *Tumor Immunology Unit, Department of Health Sciences, University of Palermo, Italy*

[3] *Molecular Targeting Unit, Department of Research, Fondazione IRCCS Istituto Nazionale dei Tumori, Milan, Italy*

[4] *Department of Medical and Biological Science, University of Udine, Italy*

[5] *Fondazione Evo ed Eldo Tempia, Biella, Italy*

Running title: Mast cells foster tumor immune suppression

Keywords: prostate cancer, mast cells, myeloid-derived suppressor cells, immune suppression, immunotherapy.

Grant support: This work was supported by grants from Fondazione Italo Monzino (to MPC) and Associazione Italiana per la Ricerca sul Cancro (I.G. n 14194 and I.G. n

18425 to MPC). EJ and AR have been awarded by Fellowships from Fondazione Umberto Veronesi

Correspondence:

Mario P. Colombo

Molecular Immunology Unit

Department of Research

Fondazione IRCCS Istituto Nazionale Tumori

via Amadeo, 42 20133 Milano, Italy

Phone: +39 0223902252 Fax: +39 0223903073

e-mail: mariopaolo.colombo@istitutotumori.mi.it

Disclosures: The authors declare no potential conflicts of interest.

Word count: 5366

The manuscript includes 7 figures, 10 supplementary figures and 2 supplementary tables.

Abbreviations' list: TRAMP (transgenic adenocarcinoma of the mouse prostate), BMMC (bone marrow-derived mast cells), rec (reconstituted), M-MDSCs (monocytic myeloid-derived suppressor cells), PMN-MDSCs (polymorphonuclear myeloid-derived suppressor cells), PIN (prostatic intraepithelial neoplasia), ADENO (adenocarcinoma), NE (neuroendocrine).

ABSTRACT

Immunotherapy, including the use of checkpoint inhibitors, is a potent therapeutic approach for some cancers, but has limited success with prostate tumors, in which immune suppression is instigated by the tumor. The immunosuppressive capacity of mast cells, which promote adenocarcinoma development in the prostate, prompted our investigation on whether mast cells promote tolerance to SV40 Large-T antigen, the transforming oncogene in transgenic adenocarcinoma of the mouse prostate (TRAMP) mice. The incidence of adenocarcinoma was reduced in the offspring of a cross between TRAMP mice and mast cell–deficient Kit^{Wsh} mice. TRAMP mice are tolerant to the SV40 Large T antigen, which is otherwise immunogenic in normal syngeneic B6 mice. Genetic ablation of mast cells in TRAMP mice restored their ability to mount a tumor-specific cytotoxic T-cell response. In Kit^{Wsh}-TRAMP mice, the restored T-cell immunity correlated with the reduced activity of polymorphonuclear myeloid-derived suppressor cells (PMN-MDSCs), along with their reduced expression of Arg1, Nos2 and Stat3. Having found that CD40L-expressing mast cells can interact *in vivo* with CD40-expressing PMN-MDSC, we then determined that only Kit^{Wsh}-TRAMP mice reconstituted with mast cells expressing CD40L could restore PMN-MDSCs suppressive functions, T cell unresponsiveness and adenocarcinoma development. Thus mast cells have an immunoregulatory effect on PMN-MDSCs activity through CD40L-CD40 interaction, favoring immunosuppression and tumor onset. In prostate cancer patients, *in silico* analyses correlated poor clinical outcomes with high expression of genes related to mast cells and PMN-MDSCs.

INTRODUCTION

Prostate cancer is a leading cause of cancer death worldwide (1). Although surgery and radiotherapy are effective for localized disease, advanced or recurrent disease treated with androgen ablation often develop into castration-resistant and metastatic disease with fatal outcomes (2).

Immunotherapy and immune checkpoint inhibitors have been tested with success in several clinical trials treating melanoma, non-small cell lung cancer and renal cell carcinoma (3), but with little success in treating prostate cancer (2). Improved understanding of the molecular mechanisms regulating immune suppression in prostate cancer should help in tailoring the immunotherapy for these patients (4).

Mast cells, innate immune cells known for their role in allergy and anaphylaxis, are also pro-angiogenic (5) and pro-tumorigenic (6,7). The amount of mast cell infiltration into human prostate cancer correlates with prognosis; mast cells may be a useful therapeutic target (8). We have shown that pharmacologic inhibition of mast cells degranulation in TRAMP mice reduces incidence and slows progression of prostate adenocarcinoma, but favors prostate tumors with neuroendocrine features (9,10). Thus, therapeutic targeting of mast cells (i.e. with imatinib (9)) could be effective against prostate adenocarcinoma if done in combination with approaches directed against neuroendocrine differentiation. The molecular mechanisms, however, are only partially explained by the fact that mast cells supply MMP-9 until the tumor becomes able at more advanced stages to produce this protease (10). Mast cells mediate immunological tolerance in several disease models, including cancer (11), possibly through interaction with other immune suppressive cell populations such as

Tregs (12) and myeloid-derived suppressor cells (MDSC) (13). Both Tregs and MDSCs are enriched in prostate cancer patients (14-16). To study the contribution of mast cells to immunosuppression during prostate adenocarcinoma development, we used the TRAMP mouse model, in which prostate epithelium transforms because of the SV40 early genes [small and large T antigens (Tag)] driven by the androgen-responsive rat probasin regulatory element. Selective Tag expression in the prostate epithelium starts at puberty (17), driving progressive development of dysplasia, prostate intraepithelial neoplasia (PIN; week 6-16), adenocarcinoma (week 16-25), and lymph node and lung metastases (week 18-30), resembling the human pathology (18). A small percentage of TRAMP mice also develop neuroendocrine prostate cancer (19), an aggressive form of disease that in patients is associated with resistance to therapies and poor prognosis (20). In the TRAMP mouse model, Tag behaves as a non-mutated tumor-associated antigen: thymic central tolerance deletes high affinity Tag-specific $CD8^+$ T cells (21), whereas low affinity Tag-specific $CD8^+$ T cells leaving the thymus experience peripheral tolerance in correlation with tumor development and Tag expression in the prostate (22).

Here we crossed TRAMP mice with mast cell-deficient Kit^{Wsh} mice (23), and tested whether the observed reduction of adenocarcinoma incidence and growth rate was related to altered immunosuppression as a consequence of mast cell deficiency. The reconstitution of Kit^{Wsh-} TRAMP mice with mast cells from $CD40L^+$ or $CD40L^-$ donors revealed CD40L-CD40–mediated crosstalk between mast cells and polymorphonuclear (PMN) MDSCs, which then suppress the tumor-specific T-cell response, thus favoring adenocarcinoma growth. We identified in human prostate cancer patients a signature of mast cell/PMN-MDSC–related genes that correlated with relapse and reduced survival.

MATERIAL AND METHODS

Mice and treatments

TRAMP mice on C57BL6/J background (C57BL/6-tgN (TRAMP)8247Ng) were kindly provided by Dr. Vincenzo Bronte (Verona University Hospital, Italy), under agreement with Dr. Norman Michael Greenberg (formerly at Fred Hutchinson Cancer Research Center, Seattle, USA), and maintained and screened according to (17). Mice deficient in mast cells [C57BL/6-KitW-sh/W-sh (Kit^{Wsh}; (23)])] were purchased from Jackson Laboratories and intercrossed over 12 generation with TRAMP mice to obtain mast cell-deficient Kit^{Wsh}-TRAMP mice. $CD40L^{-/-}$ mice (B6.129S2 – $Cd40lg^{tm1Imx}$/J) were a kind gift of Dr. Matteo Iannacone (San Raffaele Scientific Institute, Milan, Italy). Experiments were performed in accordance to Italian law (D.lgs 26/2014). Cromolyn (10 mg/kg in saline; Sigma) was administered intraperitoneally (i.p.) 5 days per week, starting at 8 weeks of age. Mice were sacrificed at 16 or 25 weeks of age.

For T-cell depletion experiments, the thymus of 16-week-old TRAMP and Kit^{Wsh}-TRAMP mice was surgically removed. The following day mice were treated i.p. with 300 μg of depleting antibodies to CD4 and CD8 and sacrificed at 25 weeks of age.

Mice reconstitution with bone marrow-derived mast cells (BMMCs)

Bone marrow precursors from C57BL6/J or $CD40L^{-/-}$ mice were cultured *in vitro* in RPMI with 20% FBS, and 20 ng/ml both SCF and IL3 (Peprotech) (10). After 4 wk, when purity was more than 90%, 5 x 10^6 BMMCs were injected i.p. into 8-week-old mice. Mast cell degranulation was evaluated by CD107a staining as described in (9).

Immunization protocol and *in vivo* cytotoxicity assay.

Dendritic cells (DCs) were prepared culturing bone marrow precursors for 7 d with 5 ng/ml of IL4 and 25 ng/ml of GM-CSF (Peprotech). On day 7, DCs were matured for 8 h with 1μg/ml LPS (Sigma), pulsed 1 h with 2 μg/ml of TAG-$IV_{404-411}$ peptide and injected (5 x 10^5 DC/mouse) i.d into the right flank of mice.

Six days later, mice were injected i.p. with 10^7 cells containing equal numbers of splenocytes labeled with 1.25 μg/ml ($CFSE^{hi}$) or 0.125 μg/ml of CFSE ($CFSE^{low}$). $CFSE^{hi}$ cells were previously pulsed 1h with $TagIV_{404-411}$ peptide. Mice were sacrificed the following day, and their splenocytes, prostates and prostate draining lymph nodes (PDLN) analyzed by flow cytometry for the evaluation of the presence of $CFSE^{hi}$ and $CFSE^{low}$ cells. Tag-specific cytolytic activity was calculated as: (percentage $CFSE^{high}$ cells) x100 / (percentage $CFSE^{low}$ cells) (22). Splenocytes of killed mice were also tested for Tag-specific IFNγ production, as described below.

Flow cytometry

Cell suspensions were obtained from mechanical disaggregation of spleen and PDLN or from digestion of prostates with collagenase IV (1600 units/ml) for 1 h at 37°C. Cells were incubated 10 min with FcR blocker and labeled for 15 min at 4°C with fluorochrome-conjugated monoclonal antibodies (mAbs) or isotype controls. All antibodies used in our study are listed in Supplementary Table S1. For intracellular detection of IFNγ, splenocytes were stimulated 4h with $TagIV_{404-411}$ peptide (1 μg/ml), adding brefeldin A (10 μg/ml) in the last 3 h (22). Cells were stained for surface markers, fixed with 2% PFA, permeabilized with saponin (0.5% in PBS) and

incubated with anti-IFNγ. Samples were acquired with BD LSRII Fortessa™ and analyzed with the Flow Jo software.

Detection of intracellular RNA levels by flow cytometry.

FACS sorted PMN-MDSCs were seeded in 24 well plates (10^5 cells/condition), alone or with wild type or $CD40L^{-/-}$ BMMCs (1:1 ratio), or with10 μg/ml of agonistic CD40 antibody or of antagonistic CD40L antibody. The following day, cells were stained with anti-CD11b and anti-cKit (Supplementary Table S1). Cells were then fixed, permeabilized and incubated with specific fluorochrome-labelled nucleotidic probes against Arg1 (Alexa647), iNos (Alexa488) and Stat3 (Alexa488), according to the PrimeFlow® RNA Assay kit protocol (eBiosciences). Positive control samples were stained with Alexa488- or Alexa 677- probes against actin. Fluorescence minus one control (FMO) were made by staining samples with all antibodies and RNA probes except one. Levels of RNA expression were measured as: (MFI of the stained samples/MFI of the FMO), within $CD11b^+$ cells.

MDSC purification and *in vitro* suppression assay

Cell suspension obtained from murine splenocytes (pools of at least 4 mice per group) were enriched for myeloid cells with the use of CD11b-magnetic microbeads (Miltenyi Biotech; cat. no. 130-049-601), then labeled with anti-mouse CD11b, Ly6G, and Ly6C (Supplementary Table S1), and sorted with a BD FACSAria™. For *in vitro* suppression assays, 10^5 naïve C57BL6 splenocytes were labeled with CFSE and cultured alone or with MDSCs at different ratios, with anti-CD3 (2 mg/mL; eBiosciences cat. no 16-0031-85) and anti-CD28 (1 mg/mL; eBiosciences cat. no. 16-0281-85) to activate lymphocytes. Proliferation of $CD4^+$ and $CD8^+$ T cells was

assessed 3 d later, evaluating CFSE dilution by flow cytometry. When indicated, BMMCs were added to the coculture in ratios equal to MDSC.

Real-Time PCR

Total RNA was extracted using the Quick RNA micro prep kit (Zymo Research). cDNA was obtained using the MultiScribe™- Reverse Transcriptase kit (Applied Biosysyems). Real-Time PCR was performed in a total volume of 20 μL using the Taqman® Universal PCR Master Mix (Applied Biosystems), 20 ng of cDNA and specific probes for Arg1, iNOS, Stat3, Tgfβ or IL6 (Applied Biosystems). Values were normalized to internal control (GAPDH) and to MDSCs from control TRAMP mouse using the ΔΔCT method.

Histology and Immunohistochemistry

Murine urogenital apparata and spleens and human tumor samples were fixed in formalin and embedded in paraffin. Sections (5 μM) were stained with H&E (BioOptica, Milan, Italy) and evaluated by a pathologist. Prostates lesions were scored as dysplasia, prostatic intraepithelial-neoplasia (PIN), adenocarcinoma (ADENO) and neuroendocrine tumor (NE). For evaluation of mast cell infiltration, sections were stained with toluidine blue (BioOptica). Immunohistochemistry was performed using the streptavidin-biotin-peroxidase complex method, and 3,3′-Diaminobenzidine tetrahydrochloride as chromogenic substrate. Antibodies used are listed in Supplementary Table 1. Slides were analyzed under an Axioscope A1 microscope equipped with Axiocam 503 Color camera (Zeiss). For tumor burden calculation, three non-overlapping panoramic microphotographs (at x50 magnification) of H&E stained slides were collected from each sample and analyzed

using the Zen 2.0 Software (Zeiss), by contouring the foci of high grade dysplasia/PIN, in situ carcinoma, and invasive carcinoma, and quantifying the extension of the relative areas (μm^2).

Immunofluorescence and confocal microscopy

Antibodies used for immunofluorescence are listed in Supplementary Table S1. Imaging was performed using a confocal laser-scanning microscope Leica TCS SP8 X (Leica Microsystems), equipped with a pulsed super continuum White Light Laser (470-670nm; 1nm tuning step size). Laser lines were 495 nm for FITC and Alexa 488, 556 nm for alexa 546 and 633 nm for APC; detection range were 501nm to 556 nm, 569 to 630 nm and 638 to 744 nm, respectively. Images were acquired in the scan format 1024x1024 pixel using a HC PL APO 63X/1.40 CS2 oil immersion objective and a pinhole set to 1 Airy unit. Data were analyzed using the software Leica LASX rel.1.1 (Leica Microsystems).

Bioinformatic Analyses

The Chiorino's dataset (GEO #GSE60329), is described in (24). For Taylor (25) and Setlur (26) datasets, data were downloaded from the GEO repository (GSE21032 and GSE8402). Samr was used to identify a gene signature associated with biochemical relapse in the Chiorino's dataset (27). Starting from a list of 90 genes specifically expressed by mast cells and PMN-MDSCs retrieved from the literature (28,29) and from the Cibersort tool (https://cibersort.stanford.edu), we obtained a list of 23 Agilent probes, corresponding to 20 unique genes, high expression of which was associated with biochemical recurrence. The ability of the signature to generate sample groups associated with survival was tested on Kaplan-Meier curves and log-

rank test. Curves and *P* values were generated with the Bioconductor package survival. Samples were divided according to the median of the average expression of the signature genes. sigCheck was used to test random signatures of the same length for each dataset, using 1000 iterations (30). An empirical *P*-value was computed based on the percentile rank of the performance of the primary signature compared to a null distribution of the performance of the random signatures.

Statistical Analyses

Statistical analyses were performed with the GraphPad Prism software (GraphPad Software, La Jolla, CA, USA); we used Fisher's Test for comparison of tumor frequencies and the Student *t* test, or One-Way ANOVA followed by Tukey's tests for other experiments.

RESULTS

Mast cell deletion restrained prostate adenocarcinoma growth in TRAMP mice.

To investigate whether mast cells support spontaneous prostate cancer occurrence, we crossed TRAMP mice with mast cell-deficient Kit^{Wsh} mice (23). We compared tumor growth and histotype between cohorts of 25 weeks old mice. As expected (17,19), the majority (80%) of observed TRAMP mice showed multifocal invasive prostate adenocarcinoma (Fig.1A and 1B), whereas a small percentage developed prostate tumor with neuroendocrine features (13%) and only few had evidence of dysplasia or prostatic intraepithelial neoplasia (PIN; 7%) (Fig.1A). Conversely, Kit^{Wsh}-TRAMP mice showed impaired adenocarcinoma growth. Adenocarcinoma occurred in only 21.4% of mice; a larger portion of the mice were afflicted only with prostate lesions that were scored as dysplasia or PIN (42.9%) (Fig. 1A and 1B). Thus, mast cells encouraged the growth of invasive prostate adenocarcinoma.

Nevertheless, as previously observed (9,10), the incidence of prostate neuroendocrine tumors increased in mast cell-deficient mice (35.7% in Kit^{Wsh}-TRAMP mice vs 13% in TRAMP mice; Fig.1A), suggesting that mast cells also prevent development of this aggressive variant. Neuroendocrine prostate cancer was identifiable at necropsy as a spherical mass overwhelming the prostate, and can also be detected by ultrasound imaging as early as 15-18 weeks of age (31). To retain our focus on the role of mast cells in immunosuppression and adenocarcinoma outgrowth, we excluded from further analysis TRAMP or Kit^{Wsh}-TRAMP mice bearing neuroendocrine prostate cancer.

Tumor-specific $CD8^+$ T cells were not inhibited without mast cells.

We investigated whether mast cell-mediated immunosuppression occurs in prostate cancer and can contribute to adenocarcinoma onset and progression. We analyzed mice at 16 weeks of age, a time when TRAMP mice have already developed peripheral $CD8^+$ T-cell tolerance against SV40 Large-T antigen (Tag) (22), which behaves as a non-mutated self tumor-associated antigen in this model (21). At this time point, both TRAMP and Kit^{Wsh}-TRAMP mice displayed similar prostatic PIN lesions (Fig. 1C) and Tag expression (Fig. 1D). Age-matched (16-week old) TRAMP, Kit^{Wsh}-TRAMP and non-oncogenic C57BL6 (B6) and Kit^{Wsh} littermates were immunized with dendritic cells (DC) pulsed with the CD8-immunodominant Tag epitope (TagIV; (32)) and killed one week later to test *in vivo* Tag-specific cytotoxic activity (Supplementary Fig. S1A) and *ex vivo* IFNγ production by $CD8^+$ T cells (Supplementary Fig. S1B). Consistent with previously published data (22), we detected negligible *in vivo* Tag-specific cytotoxicity in both spleen (30.3 % ± 11.70, Fig. 1E) and prostate-draining lymph nodes (PDLN) of TRAMP mice (29.89 % ± 7.81, Supplementary Fig. S2A). TRAMP mice also showed barley detectable *ex-vivo* Tag-specific IFNγ production by $CD8^+$ T cells isolated from spleen (0.19% ± 0.18, Fig. 1F), PDLN (17.8% ± 1.31, Supplementary Fig. S2B) or prostates (20. 94% ± 0.18, Supplementary Fig. S2C). On the other hand, Tag-specific cytotoxic T-cell response and IFNγ production by $CD8^+$ T cells from Kit^{Wsh}-TRAMP mice were almost comparable to that of T cells of B6 mice used as positive control upon immunization with the same vaccine both in spleen (cytotoxicity 67.81 % ± 15.17 vs 86.25 % ± 8.33, Fig. 1E; and IFNγ production 1.06 % ± 0.30 vs 1.82 % ± 0.24, Fig. 1F) and PDLN (cytotoxicity 68.33 % ± 14.53 vs 81.25 % ± 17.56, Supplementary Fig. S2A; and IFNγ production 7.29 % ± 0.66 vs 8.43 % ± 2.11, Supplementary Fig S2B). $CD8^+$ T cells infiltrating the prostates of Kit^{Wsh}-TRAMP mice released

significantly increased amounts of IFNγ compared with $CD8^+$ T cells from prostates of TRAMP mice (30.39 % ± 9.68 vs 20.94 % ± 3.83, Supplementary Fig. S2C). These results indicate that in absence of mast cells, tumor-specific $CD8^+$ T cells became manifest, both systemically and within the tumor microenvironment.

Addition of mast cells restored $CD8^+$ T-cell unresponsiveness and tumor growth. To confirm the involvement of mast cells in inhibiting tumor-specific $CD8^+$ T cells and in supporting prostate adenocarcinoma growth, we reconstituted 8-week old Kit^{Wsh}-TRAMP mice with bone marrow-derived mast cells (BMMCs). We analyzed the mice 8 weeks later for Tag- specific $CD8^+$ T-cell activity. Histologic sections of spleens and prostates stained with toluidine blue showed correct repopulation and distribution of mast cells in reconstituted Kit^{Wsh}-TRAMP mice (Fig. 2A and Supplementary Fig. S3A). In reconstituted Kit^{Wsh}-TRAMP mice, both *in vivo* Tag-specific cytotoxicity and *ex-vivo* IFNγ production by $CD8^+$ T cells was lowered to that of TRAMP mice (0.30 % ± 0.32 vs 0.40 % ± 0.33, Fig. 2B, and 61.80 % ± 19.40 vs 62.91 % ± 26.94, Fig. 2C, respectively). Consistent with the inverse correlation between effective $CD8^+$ T-cell activity and frequency of adenocarcinoma, 60% of Kit^{Wsh}-TRAMP mice reconstituted with BMMCs developed adenocarcinomas, whereas only 21.4% of non-reconstituted mice developed adenocarcinomas (Fig. 2D). To further confirm the link between effective tumor specific T-cell function and reduced adenocarcinoma growth occurring in Kit^{Wsh}-TRAMP mice, we depleted in vivo both $CD4^+$ and $CD8^+$ T lymphocytes, by surgical removal of thymus followed by administration of specific depleting antibodies (Supplementary Fig. S3B). In T cell-depleted Kit^{Wsh}-TRAMP mice, the frequency of infiltrating adenocarcinoma raised up to levels comparable to TRAMP mice (Fig 2E and 2F). On the contrary,

adenocarcinoma growth was unaltered in TRAMP mice regardless of whether or not T cells were depleted (Fig 2E and 2F), a result consistent with the unresponsiveness of tumor-specific T cells in these mice (Fig.1E, 1F, 2B and 2C and [(22)]). Thus, mast cells impair tumor-specific $CD8^+$ T-cell activity allowing growth of adenocarcinoma in TRAMP mice.

Mast cells support PMN-MDSC suppressive activity.

To exclude the possibility that increased antitumor immune response in Kit^{Wsh}-TRAMP mice could have been due to altered T-cell frequency or distribution, we evaluated by flow cytometry the percentages of T lymphocytes in spleens and prostates of TRAMP, Kit^{Wsh}-TRAMP, Kit^{Wsh}-TRAMP mice reconstituted with BMMCs and their non-oncogenic littermates (Supplementary Fig. S4). The frequency of $CD8^+$ T cells in the spleen was lower in Kit^{Wsh}-TRAMP or in reconstituted Kit^{Wsh}-TRAMP mice than in TRAMP mice, excluding an expansion of $CD8^+$ T cells in the absence of mast cells. No differences in $CD4^+$ and $CD8^+$ T cells infiltrating the prostates were noted among the different strains (Supplementary Fig. S4).
Data collected so far indicate that mast cells can hamper tumor-specific $CD8^+$ T-cell responses both systemically and at the tumor site, through either direct or indirect interactions between mast cells and T cells. Immunofluorescence analysis excluded direct interaction between mast cells and T cells by revealing that in the spleen of TRAMP mice, mast cells are not present in the splenic white pulp and do not co-localize with CD3-expressing cells (Fig. 3A). On the contrary we found mast cells within the splenic red pulp, in close contact with $Gr1^{hi}$ cells (Fig. 3A). Gr1 antibodies (recognizing both Ly6C and Ly6G epitopes) could identify myeloid-derived suppressor cells (MDSCs), which accumulate in the spleen of tumor bearing mice

(33). Mast cells can enhance MDSCs suppressive activity (13,34). Therefore we tested whether the increased tumor-specific $CD8^+$ T-cell response in mast cell-deficient Kit^{Wsh}-TRAMP mice correlated with reduced MDSCs activity. The characteristic expansion of immature $CD11b^+Ly6G^{int}Ly6C^{int}$ cells that occurs in Kit^{Wsh} mice (35,36) was evident also in the spleen of Kit^{Wsh}-TRAMP mice (Supplementary Figs. S5A and S5B), which also showed more monocytic (M-) MDSC–like cells ($CD11b^+Ly6G^{low}Ly6C^{hi}$) and polymorphonuclear (PNM-) MDSCs ($CD11b^+Ly6G^{hi}Ly6C^{low}$) (Supplementary Figs. S5A and 5B). On the contrary, no differences in the frequencies of M-MDSCs and PMN-MDSCs were detected in the prostates of Kit^{Wsh}-TRAMP vs TRAMP mice.(Supplementary Figs. S5A and 5B). We sorted M-MDSC- like cells and PMN-MDSCs from the spleen of 16-week old TRAMP and Kit^{Wsh}-TRAMP mice with a FACS, and tested them for the ability to suppress $CD4^+$ and $CD8^+$ T-cell proliferation. No M-MDSC-like cells from any of the strains had suppressive activity (Fig. 3B, upper panels). On the contrary, PMN-MDSCs were suppressive when from TRAMP mice, but less suppressive when they were from Kit^{Wsh}-TRAMP mice (Fig. 3B, lower panels). The reduced function of PMN-MDSCs from Kit^{Wsh}-TRAMP mice paralleled decreased transcript levels of Arg1, iNOS, and Stat-3, which all promote MDSC suppressive activity (Fig. 3C). Conversely, little TGFβ and IL6 were expressed and their RNA level in PMN-MDSCs from both TRAMP and Kit^{Wsh}-TRAMP mice was similar (Fig 3C). Thus, mast cells can interact with PMN-MDSCs to increase their suppressive ability.

Interaction with PMN-MDSCs not dependent on soluble factors from mast cells.

To investigate the mechanism used by mast cells to enhance PMN-MDSC suppression, we considered their release of soluble mediators (37), and treated

TRAMP mice with the mast cells stabilizer Cromolyn, which blocks mast cell degranulation. Treatment had no effect on Tag-specific $CD8^+$ T-cell responses (Fig. 4A and 4B) (9,10), but partially inhibited adenocarcinoma growth and increased the frequency of neuroendocrine tumors (adenocarcinoma frequency was 50% in Cromolyn-treated TRAMP mice, 80% in TRAMP mice, and 21.4% in Kit^{Wsh}-TRAMP mice; Fig. 4C). We concluded that soluble factors were not necessary for mast cell:PMN-MDSC crosstalk, and that immunosuppression may instead depend on receptor-ligand interaction.

Mast cell CD40L triggered PMN-MDSC CD40 to suppress T-cell function.

CD40 has been already associated to MDSC suppression (38) and to their interaction with mast cells, at least *in vitro* (13). We confirmed CD40L expression on BM-derived mast cells cultured *in vitro* (Supplementary Fig. S6A), and on mast cells isolated from the spleen of TRAMP mice (Supplementary Fig. S6B). PMN-MDSCs isolated from the same spleens showed positivity for CD40 (Supplementary Fig. S6C). The co-localization between mast cells and CD40 in the spleen of TRAMP mice was visualized by triple immunofluorescence with Gr1, CD40 and the mast cells-marker Tryptase (Fig. 5A). No mast cells were found to co-localize with $CD40^{hi}$ B cells in the splenic follicular zone (Supplementary Fig. S6D).

To further confirm the role of the CD40L-CD40 axis in the interaction between mast cells and PMN-MDSCs, we reconstituted Kit^{Wsh}-TRAMP mice with BMMCs obtained from either wild-type or $CD40L^{-/-}$ mice and tested the suppressive activity of PMN-MDSCs (Fig. 5B). Wild-type and $CD40L^{-/-}$ mast cells differentiated and matured *in vitro* similarly, were equally responsive to stimuli (Supplementary Figs. S7A and 7B), and were similarly recruited to spleen and prostates in Kit^{Wsh}-TRAMP

mice after *in vivo* reconstitution (Supplementary Fig. S7C). Their distribution in proximity of $Gr1^+$ cells in the spleen of reconstituted Kit^{Wsh}-TRAMP mice was also comparable (Supplementary Fig. S7D). Reconstitution with wild-type BMMCs restored PMN-MDSC suppressive activity, but reconstitution with $CD40L^{-/-}$ mast cells did not (Fig. 5B). The expression of Arg1, iNOS, and Stat3 in PMN-MDSCs was recovered in PMN-MDSCs from Kit^{Wsh}-TRAMP mice that received wild-type BMMCs, but not in mice that received $CD40L^{-/-}$ BMMCs (Fig. 5C). To confirm the capacity of mast cells to enhance PMN-MDSC function via CD40L-CD40 crosstalk, we performed suppressive assays, coculturing responder T cells, PMN-MDSC, and $CD40L^+$ or $CD40L^-$mast cells, either with or without antagonistic CD40L antibody. T-cell inhibition by PMN-MDSCs isolated from TRAMP mice was not further increased by the presence of mast cells, likely because of *in vivo* triggering of their CD40 signaling by splenic mast cells. In contrast, the suppressive ability of PMN-MDSCs isolated from Kit^{Wsh}-TRAMP mice cocultured with wild-type, but not $CD40L^{-/-}$, mast cells was comparable to that of TRAMP-derived PMN-MDSCs. This increase in PMN-MDSC suppressive function was partially inhibited by adding a blocking antibody to CD40L (Supplementary Fig. S7E).

To prove that CD40 triggering on PMN-MDSCs modulates Arg1, iNOS and Stat3 expression, FACS-sorted PMN-MDSCs from the spleen of Kit^{Wsh}-TRAMP mice were stimulated overnight with an agonistic anti-CD40 or cocultured with wild type or $CD40L^{-/-}$ BMMCs, either with or without antagonistic anti-CD40L. Amounts of mRNA encoding Arg1, iNOS and Stat3 were measured using the Prime Flow Assay (eBiosciences), which couples intracellular RNA detection in single cells with protein measurement by flow cytometry analysis. With this technique, we detected intracellular RNA levels, measured as mean fluorescence intensity, within the gate of

PMN-MDSCs from *in vitro* cultures (Fig. 5D, upper panels). Direct CD40 stimulation increased Arg1, iNOS and Stat3 transcripts as much or more than did stimulation with IL4 plus IFNγ, which we used as positive control (39). A similar increase was observed when PMN-MDSCs were cocultured in the presence of BMMCs. The response was blunted if antagonistic anti-CD40L was given or if BMMCs were from $CD40L^{-/-}$ mice (Fig 5D, lower panels). Thus, mast cells partner with PMN-MDSCs to instigate suppressive activity via CD40L-CD40 crosstalk.

These results were consistent with the Tag-specific response observed in Kit^{Wsh}-TRAMP mice that, although impaired by reconstitution with wild-type, $CD40L^{+}$, mast cells (Fig. 6A and 6B and Supplementary Figs. S7, F-H), remained unaltered by mast cells reconstitution with BMMCs from $CD40L^{-/-}$ mice. According to data on T-cell function, adenocarcinoma burden in Kit^{Wsh}-TRAMP mice reconstituted with $CD40L^{-/-}$ BMMCs was significantly reduced (17.2% in situ and 10.3% infiltrating adenocarcinoma on total tumor burden, respectively) in comparison to TRAMP (17.2% in situ and 78.5% infiltrating adenocarcinoma) and to Kit^{Wsh}-TRAMP mice reconstituted with wild type BMMCs (28.1% in situ and 57.2% infiltrating adenocarcinoma; Fig. 6C and 6D), and it was even lower in comparison to unreconstituted Kit^{Wsh}-TRAMP mice (40.36% in situ and 30.11% infiltrating adenocarcinoma), (Fig. 6C and 6D). These results indicate that expression of CD40L on mast cells support their crosstalk with PMN-MDSC, favoring immune escape and adenocarcinoma development, but also suggest that other mechanisms dependent on CD40L expression on mast cells could be necessary for adenocarcinoma growth.

Mast cell/PMN-MDSC gene signature associated with poor outcome in patients.

We have previously shown that in human prostate cancer, mast cells accumulate in well-differentiated tumors more than in poorly differentiated areas prone to neuroendocrine differentiation (10). Here we show, with immunohistochemistry on serial sections of human prostate cancer samples, the presence of cells positive for tryptase, CD40L, or CD33 (used as a myeloid cell marker; Supplementary Fig. S8A) in well-differentiated areas. Immunofluorescence confirmed co-expression of tryptase and CD40L on tumor infiltrating mast cells, and proximity of mast cells to $CD33^+$ cells (Supplementary Fig. S8B and C). To test the translational relevance of our finding, we applied *in silico analyses* to data sets of prostate cancer patients to look for correlation between the expression of genes characterizing mast cells and PMN-MDSCs (Supplementary Table S2) and clinical outcome. The testing data set comprised 54 primary prostate cancers associated with patients' follow up for biochemical relapse (Chiorino's dataset; (24)). A total of 23 probes, corresponding to 20 up-regulated genes, selected from the list of Supplementary Table S1 were statistically associated with higher biochemical recurrence ($P < 0.001$; Fig. 7A). These results were consistent with a publicly available dataset of 140 prostate cancer samples (Taylor's dataset; ref (25)), in which the highest expression of genes belonging to the mast cell/PMN-MDSC signature correlated with biochemical relapse ($P = 0.00467$; Fig. 7B). In both data sets, we found a positive correlation between mast cell-genes and genes related to MDSC-suppressive function (Supplementary Fig. S9). To investigate the association with overall survival, we explored Setlur's dataset comprising 358 PCa samples (26), and found a statistically significant inverse correlation of this gene signature with survival ($P = 0.00512$; Fig. 7C). The performance of this signature was tested against 1000 random gene signatures of the same length for each of the three datasets with sigCheck, leading to statistically

significant results for all of them ($P < 0.05$, Supplementary Fig. S10). Since the three datasets-derived from microarray gene expression analysis were derived from different platforms, the original 20-gene signature used for Chiorino's dataset was only partially present in the other two datasets. The gene overlap and the signatures tested for each dataset are reported in Fig. 7D. These results indicate that concomitant upregulation of mast cell– and PMN-MDSC–related genes negatively correlates with clinical outcome of prostate cancer patients.

DISCUSSIO(N

Prostate cancer remains one of the cancers most refractory to immunotherapy, including checkpoint inhibitors (4). A deeper understanding of the immunosuppressive networks established at the time of tumor development is necessary to fight this disease.

We have previously identified mast cells as key stromal accomplices in prostate cancer, capable of influencing the balance between adenocarcinoma and neuroendocrine histotypes (9,10). Our data showing increase in the frequency of neuroendocrine tumors after pharmacologic inhibition of mast cell degranulation ((9,10) and this paper) indicate that mast cells can protect against emergence of neuroendocrine prostate cancer, most likely through release of as yet unidentified soluble factors. Mast cells can also foster the growth of prostate adenocarcinoma, at least partially due to their provision of MMP9, until the tumor becomes capable of its own MMP9 production during progression (10). However, adenocarcinoma formation was only moderately restrained in TRAMP mice pharmacologically treated to block mast cell degranulation ((9,10) and this paper). This suggests that other mechanisms implying interaction of mast cells with other cell types, through surface receptor-ligand pairs, might foster prostate adenocarcinoma.

Thus our work shows that mast cells contribute to prostate adenocarcinoma through the suppression of antitumor T-cell responses, which in turn control onset and growth extent of adenocarcinoma. Immunosuppression was mediated by direct interactions between mast cells and PMN-MDSCs via CD40L-CD40 engagement, which resulted in enhanced PMN-MDSC suppressive activity.

Mast cells can augment MDSC suppressive functions (13,34) and these cells can interact by binding of CD40L and CD40, at least *in vitro* (13). Other than confirming that CD40 expression is required for MDSC activity (38), our *in vivo* results show that mast cells interact with PMN-MDSCs through CD40L-CD40 signaling in the spleen of tumor-bearing mice, which results in suppression of tumor-specific T cells and unrestrained tumor growth. Depletion of mast cells or interference with the CD40L-CD40 interaction restored the $CD8^+$ T-cell response and reduced tumor growth. Once stimulated by mast cells, PMN-MDSCs could mediate T-cell suppression directly in the spleen (40) or through migration to lymph nodes or the tumor site.

Adenocarcinoma burden was lower in Kit^{Wsh}-TRAMP mice reconstituted with $CD40L^{-/-}$ BMMCs than in Kit^{Wsh}-TRAMP mice lacking mast cells, suggesting that other pro-tumor functions of mast cells, perhaps related to cytokines or MMP release, could be fostered by reverse CD40L signaling (13,41). Although several other myeloid cell types express CD40, mast cells selectively engaged with PMN-MDSCs, an issue that deserves further investigation.

Abnormal myelopoiesis leading to increased accumulation of immature granulocytic precursors ($CD11b^+Ly6G^{low}Ly6C^{low}$) has been described in Kit^{Wsh} mice, especially on a mixed (BALB/c x C57BL6)F1 background (36). This $CD11b^+Ly6G^{int}Ly6C^{low}$ population is distinct from canonical $CD11b^+Ly6G^{hi}Ly6C^{low}$ PMN-MDSCs and $CD11b^+Ly6G^{low}Ly6C^{hi}$ M-MDSCs. $CD11b^+Ly6G^{int}Ly6C^{low}$ cells seem to accumulate regardless of mast cell presence, responding instead to an inversion of the cKit gene promoter (23). Indeed, we found in spleen of Kit^{Wsh}-TRAMP mice an accumulation of $CD11b^+Ly6G^{int}Ly6C^{int}$ cells (2.87% ± 2.06 of $CD45^+$ cells), which were very low in TRAMP mice (0.32% ± 0.28 of $CD45^+$ cells). The frequency of these immature $CD11b^+Ly6G^{int}Ly6C^{int}$ myeloid cells was unaltered by reconstitution of Kit^{Wsh}-

TRAMP mice with BMMCs. We also observed more $CD11b^{+}Ly6G^{low}Ly6C^{hi}$ M-MDSC-like cells and $CD11b^{+}Ly6G^{hi}Ly6C^{low}$ PMN-MDSCs. Nevertheless, systemic reconstitution of Kit^{Wsh} mice with BMMCs corrects the mast cell defect and allows testing of specific mast cell functions in these mice (10,23). Given that reconstitution of Kit^{Wsh}-TRAMP mice with wild-type or $CD40L^{-/-}$BMMCs induced different outcomes in term of PMN-MDSCs activity, tumor-specific $CD8^{+}$ T-cell suppression and adenocarcinoma growth, we conclude that mast cells do interact with MDSCs in tumor-bearing mice, and that our results are not an artifact due to the intrinsic limitations of this murine model.

In our prostate cancer model, we found that only PMN-MDSCs were endowed with T-cell suppressive ability. In prostate cancer patients, accumulation of both $CD14^{+}$HLA-DR^{-} M-MDSCs and $CD15^{+}CD33^{low}$ PMN-MDSCs has been reported (14,15). *In silico* analyses corroborated our results in the TRAMP model showing that the mast cell/PMN-MDSC gene signature correlated with biochemical relapse and reduced survival of prostate cancer patients. Indeed, another study reported that peripheral blood of either metastatic breast or prostate cancer patients shows accumulation of $CD33^{+}$HLA-DR^{-} cells ("early-stage" MDSCs (33)), which expressed CD40 (42). In the same study, increased amounts of soluble CD40L were detected in the serum of the patients (42). Those data raised the question of whether the CD40L-CD40 pathway might be detrimental, inducing immune suppression rather than immune stimulation, in certain clinical settings (42). Consistent with this idea, in a clinical trial evaluating the efficacy of a viral vaccine against prostate cancer (PROSTVAC®), higher serum levels of soluble CD40L correlated with reduced patient survival (43).

Our data suggest that CD40L-CD40 signaling may sustain immune suppression in those cancer patients characterized by accumulation of both mast cells and MDSCs. This observation might inform design of immunotherapies. Patients should be screened for the accumulation of mast cells and MDSCs before immunotherapy with agonistic CD40 antibodies (44), which our results indicate could be detrimental. On the other hand, blocking CD40L-CD40 interaction with antagonistic CD40 antibodies, such as Lucatumumab (Novartis) (44), may increase the antitumor immune response, and might be a therapeutic addition that could be tested in combination with checkpoint inhibitors or other immunotherapies.

ACKNOWLEDGMENTS

We thank from INT: Ivano Arioli, Laura Botti, Renata Ferri and Mariella Parenza for technical assistance, Ester Grande for administrative assistance and Ivan Muradore and Gabriella Abolafio for Cell Sorting. We thank Dr. Matteo Iannacone from San Raffaele Scientific Institute for having provided $CD40L^{-/-}$ mice. Valeria Cancila, PhD student is supported, for this research, by the University of Palermo (IT), Doctoral Course of Experimental Oncology and Surgery, Cycle XXXI

REFERENCES

1. Jemal A, Bray F, Center MM, Ferlay J, Ward E, Forman D. Global cancer statistics. CA: a cancer journal for clinicians **2011**;61(2):69-90 doi 10.3322/caac.20107.
2. Saad F, Miller K. Current and Emerging Immunotherapies for Castration-resistant Prostate Cancer. Urology **2015**;85(5):976-86 doi 10.1016/j.urology.2014.12.029.
3. Topalian SL, Drake CG, Pardoll DM. Immune checkpoint blockade: a common denominator approach to cancer therapy. Cancer Cell **2015**;27(4):450-61 doi 10.1016/j.ccell.2015.03.001.
4. Burotto M, Singh N, Heery CR, Gulley JL, Madan RA. Exploiting synergy: immune-based combinations in the treatment of prostate cancer. Front Oncol **2014**;4:351 doi 10.3389/fonc.2014.00351.
5. Coussens LM, Raymond WW, Bergers G, Laig-Webster M, Behrendtsen O, Werb Z*, et al.* Inflammatory mast cells up-regulate angiogenesis during squamous epithelial carcinogenesis. Genes & development **1999**;13(11):1382-97.
6. Chang DZ, Ma Y, Ji B, Wang H, Deng D, Liu Y*, et al.* Mast cells in tumor microenvironment promotes the in vivo growth of pancreatic ductal adenocarcinoma. Clin Cancer Res **2011**;17(22):7015-23 doi 10.1158/1078-0432.CCR-11-0607.
7. Ma Y, Hwang RF, Logsdon CD, Ullrich SE. Dynamic mast cell-stromal cell interactions promote growth of pancreatic cancer. Cancer Res **2013**;73(13):3927-37 doi 10.1158/0008-5472.CAN-12-4479.
8. Johansson A, Rudolfsson S, Hammarsten P, Halin S, Pietras K, Jones J*, et al.* Mast cells are novel independent prognostic markers in prostate cancer and represent a target for therapy. Am J Pathol **2010**;177(2):1031-41 doi 10.2353/ajpath.2010.100070.
9. Jachetti E, Rigoni A, Bongiovanni L, Arioli I, Botti L, Parenza M*, et al.* Imatinib Spares cKit-Expressing Prostate Neuroendocrine Tumors, whereas Kills Seminal Vesicle Epithelial-Stromal Tumors by Targeting PDGFR-beta. Mol Cancer Ther **2017**;16(2):365-75 doi 10.1158/1535-7163.MCT-16-0466.
10. Pittoni P, Tripodo C, Piconese S, Mauri G, Parenza M, Rigoni A*, et al.* Mast cell targeting hampers prostate adenocarcinoma development but promotes the occurrence of highly malignant neuroendocrine cancers. Cancer Res **2011**;71(18):5987-97 doi 10.1158/0008-5472.CAN-11-1637.
11. Nowak EC, de Vries VC, Wasiuk A, Ahonen C, Bennett KA, Le Mercier I*, et al.* Tryptophan hydroxylase-1 regulates immune tolerance and inflammation. J Exp Med **2012**;209(11):2127-35 doi 10.1084/jem.20120408.

12. Lu LF, Lind EF, Gondek DC, Bennett KA, Gleeson MW, Pino-Lagos K*, et al.* Mast cells are essential intermediaries in regulatory T-cell tolerance. Nature **2006**;442(7106):997-1002 doi 10.1038/nature05010.
13. Danelli L, Frossi B, Gri G, Mion F, Guarnotta C, Bongiovanni L*, et al.* Mast cells boost myeloid-derived suppressor cell activity and contribute to the development of tumor-favoring microenvironment. Cancer Immunol Res **2015**;3(1):85-95 doi 10.1158/2326-6066.CIR-14-0102.
14. Hossain DM, Pal SK, Moreira D, Duttagupta P, Zhang Q, Won H*, et al.* TLR9-Targeted STAT3 Silencing Abrogates Immunosuppressive Activity of Myeloid-Derived Suppressor Cells from Prostate Cancer Patients. Clin Cancer Res **2015**;21(16):3771-82 doi 10.1158/1078-0432.CCR-14-3145.
15. Idorn M, Kollgaard T, Kongsted P, Sengelov L, Thor Straten P. Correlation between frequencies of blood monocytic myeloid-derived suppressor cells, regulatory T cells and negative prognostic markers in patients with castration-resistant metastatic prostate cancer. Cancer Immunol Immunother **2014**;63(11):1177-87 doi 10.1007/s00262-014-1591-2.
16. Sorrentino C, Musiani P, Pompa P, Cipollone G, Di Carlo E. Androgen deprivation boosts prostatic infiltration of cytotoxic and regulatory T lymphocytes and has no effect on disease-free survival in prostate cancer patients. Clin Cancer Res **2011**;17(6):1571-81 doi 10.1158/1078-0432.CCR-10-2804.
17. Greenberg NM, DeMayo F, Finegold MJ, Medina D, Tilley WD, Aspinall JO*, et al.* Prostate cancer in a transgenic mouse. Proc Natl Acad Sci U S A **1995**;92(8):3439-43.
18. Shappell SB, Thomas GV, Roberts RL, Herbert R, Ittmann MM, Rubin MA*, et al.* Prostate pathology of genetically engineered mice: definitions and classification. The consensus report from the Bar Harbor meeting of the Mouse Models of Human Cancer Consortium Prostate Pathology Committee. Cancer Res **2004**;64(6):2270-305.
19. Chiaverotti T, Couto SS, Donjacour A, Mao JH, Nagase H, Cardiff RD*, et al.* Dissociation of epithelial and neuroendocrine carcinoma lineages in the transgenic adenocarcinoma of mouse prostate model of prostate cancer. Am J Pathol **2008**;172(1):236-46 doi 10.2353/ajpath.2008.070602.
20. Terry S, Beltran H. The many faces of neuroendocrine differentiation in prostate cancer progression. Front Oncol **2014**;4:60 doi 10.3389/fonc.2014.00060.
21. Zheng X, Gao JX, Zhang H, Geiger TL, Liu Y, Zheng P. Clonal deletion of simian virus 40 large T antigen-specific T cells in the transgenic adenocarcinoma of mouse prostate mice: an important role for clonal deletion in shaping the repertoire of T cells specific for antigens overexpressed in solid tumors. J Immunol **2002**;169(9):4761-9.
22. Degl'Innocenti E, Grioni M, Boni A, Camporeale A, Bertilaccio MT, Freschi M*, et al.* Peripheral T cell tolerance occurs early during spontaneous prostate cancer development and can be rescued by dendritic cell immunization. Eur J Immunol **2005**;35(1):66-75 doi 10.1002/eji.200425531.
23. Grimbaldeston MA, Chen CC, Piliponsky AM, Tsai M, Tam SY, Galli SJ. Mast cell-deficient W-sash c-kit mutant Kit W-sh/W-sh mice as a model for

investigating mast cell biology in vivo. Am J Pathol **2005**;167(3):835-48 doi 10.1016/S0002-9440(10)62055-X.

24. Lefort K, Ostano P, Mello-Grand M, Calpini V, Scatolini M, Farsetti A*, et al.* Dual tumor suppressing and promoting function of Notch1 signaling in human prostate cancer. Oncotarget **2016**;7(30):48011-26 doi 10.18632/oncotarget.10333.
25. Taylor BS, Schultz N, Hieronymus H, Gopalan A, Xiao Y, Carver BS*, et al.* Integrative genomic profiling of human prostate cancer. Cancer Cell **2010**;18(1):11-22 doi 10.1016/j.ccr.2010.05.026.
26. Setlur SR, Mertz KD, Hoshida Y, Demichelis F, Lupien M, Perner S*, et al.* Estrogen-dependent signaling in a molecularly distinct subclass of aggressive prostate cancer. J Natl Cancer Inst **2008**;100(11):815-25 doi 10.1093/jnci/djn150.
27. Tusher VG, Tibshirani R, Chu G. Significance analysis of microarrays applied to the ionizing radiation response. Proc Natl Acad Sci U S A **2001**;98(9):5116-21 doi 10.1073/pnas.091062498.
28. Motakis E, Guhl S, Ishizu Y, Itoh M, Kawaji H, de Hoon M*, et al.* Redefinition of the human mast cell transcriptome by deep-CAGE sequencing. Blood **2014**;123(17):e58-67 doi 10.1182/blood-2013-02-483792.
29. Youn JI, Collazo M, Shalova IN, Biswas SK, Gabrilovich DI. Characterization of the nature of granulocytic myeloid-derived suppressor cells in tumor-bearing mice. J Leukoc Biol **2012**;91(1):167-81 doi 10.1189/jlb.0311177.
30. J SRaN. 2017 SigCheck: Check a gene signature's prognostic performance against random signatures, known signatures, and permuted data/metadata. . R package version 2.8.0.
31. Mauri G, Jachetti E, Comuzzi B, Dugo M, Arioli I, Miotti S*, et al.* Genetic deletion of osteopontin in TRAMP mice skews prostate carcinogenesis from adenocarcinoma to aggressive human-like neuroendocrine cancers. Oncotarget **2016**;7(4):3905-20 doi 10.18632/oncotarget.6678.
32. Mylin LM, Bonneau RH, Lippolis JD, Tevethia SS. Hierarchy among multiple H-2b-restricted cytotoxic T-lymphocyte epitopes within simian virus 40 T antigen. J Virol **1995**;69(11):6665-77.
33. Bronte V, Brandau S, Chen SH, Colombo MP, Frey AB, Greten TF*, et al.* Recommendations for myeloid-derived suppressor cell nomenclature and characterization standards. Nat Commun **2016**;7:12150 doi 10.1038/ncomms12150.
34. Saleem SJ, Martin RK, Morales JK, Sturgill JL, Gibb DR, Graham L*, et al.* Cutting edge: mast cells critically augment myeloid-derived suppressor cell activity. J Immunol **2012**;189(2):511-5 doi 10.4049/jimmunol.1200647.
35. Nigrovic PA, Gray DH, Jones T, Hallgren J, Kuo FC, Chaletzky B*, et al.* Genetic inversion in mast cell-deficient (Wsh) mice interrupts corin and manifests as hematopoietic and cardiac aberrancy. Am J Pathol **2008**;173(6):1693-701 doi 10.2353/ajpath.2008.080407.
36. Michel A, Schuler A, Friedrich P, Doner F, Bopp T, Radsak M*, et al.* Mast cell-deficient Kit(W-sh) "Sash" mutant mice display aberrant myelopoiesis leading to the accumulation of splenocytes that act as myeloid-derived suppressor cells. J Immunol **2013**;190(11):5534-44 doi 10.4049/jimmunol.1203355.

37. Rigoni A, Colombo MP, Pucillo C. The Role of Mast Cells in Molding the Tumor Microenvironment. Cancer Microenviron **2014** doi 10.1007/s12307-014-0152-8.
38. Pan PY, Ma G, Weber KJ, Ozao-Choy J, Wang G, Yin B*, et al.* Immune stimulatory receptor CD40 is required for T-cell suppression and T regulatory cell activation mediated by myeloid-derived suppressor cells in cancer. Cancer Res **2010**;70(1):99-108 doi 10.1158/0008-5472.CAN-09-1882.
39. Angulo I, Rullas J, Campillo JA, Obregon E, Heath A, Howard M*, et al.* Early myeloid cells are high producers of nitric oxide upon CD40 plus IFN-gamma stimulation through a mechanism dependent on endogenous TNF-alpha and IL-1alpha. Eur J Immunol **2000**;30(5):1263-71 doi 10.1002/(SICI)1521-4141(200005)30:5<1263::AID-IMMU1263>3.0.CO;2-5.
40. Ugel S, Peranzoni E, Desantis G, Chioda M, Walter S, Weinschenk T*, et al.* Immune tolerance to tumor antigens occurs in a specialized environment of the spleen. Cell Rep **2012**;2(3):628-39 doi 10.1016/j.celrep.2012.08.006.
41. Eissner G, Kolch W, Scheurich P. Ligands working as receptors: reverse signaling by members of the TNF superfamily enhance the plasticity of the immune system. Cytokine Growth Factor Rev **2004**;15(5):353-66 doi 10.1016/j.cytogfr.2004.03.011.
42. Huang J, Jochems C, Talaie T, Anderson A, Jales A, Tsang KY*, et al.* Elevated serum soluble CD40 ligand in cancer patients may play an immunosuppressive role. Blood **2012**;120(15):3030-8 doi 10.1182/blood-2012-05-427799.
43. Gulley JL, Arlen PM, Madan RA, Tsang KY, Pazdur MP, Skarupa L*, et al.* Immunologic and prognostic factors associated with overall survival employing a poxviral-based PSA vaccine in metastatic castrate-resistant prostate cancer. Cancer Immunol Immunother **2010**;59(5):663-74 doi 10.1007/s00262-009-0782-8.
44. Vonderheide RH, Glennie MJ. Agonistic CD40 antibodies and cancer therapy. Clin Cancer Res **2013**;19(5):1035-43 doi 10.1158/1078-0432.CCR-12-2064.

FIGURE LEGENDS

Figure 1. Mast cell-deficient Kit^{Wsh}-TRAMP mice have lower incidence of adenocarcinoma and maintain systemic tumor specific T-cell response. A) Graph depicts the relative percentage of dysplasia/PIN, adenocarcinoma (ADENO) or neuroendocrine (NE) lesions in 25 weeks old TRAMP (n = 17) and Kit^{Wsh}-TRAMP mice (n = 15), as scored by a pathologist. Fisher's test: **** $P < 0.0001$. B) Representative hematoxilin and eosin staining of prostates of 25-week-old TRAMP and Kit^{Wsh}-TRAMP mice affected by adenocarcinoma or PIN, respectively. Magnification 20X. C-D) Representative hematoxilin and eosin (C), or Tag staining (D), of prostates of 16-week-old TRAMP and Kit^{Wsh}-TRAMP mice. Magnification 20X. E) 16 weeks old TRAMP, Kit^{Wsh}-TRAMP and control nontumor bearing C57BL6 (B6) and Kit^{Wsh} mice were immunized with DC pulsed with TagIV peptide. One week later, *in vivo* cytotoxicity was tested as described in Materials and Methods. F) Splenocytes of the animals described in (D) were also stimulated for 4h with TagIV, or left untreated, in the presence of brefeldin A, and tested for IFNγ production by intracellular staining and flow cytometry. Histogram reports the quantification of IFNγ production by TagIV stimulated CD8$^+$ T cells. Values are subtracted of background, i.e. spontaneous IFNγ release by unstimulated CD8$^+$ T cells. Naive: non-immunized control mice. Experiment was repeated three times with at least 4 mice per group. Anova followed by Tukey's test: * $P < 0.05$, ** $P < 0.01$, *** $P < 0.001$.

Figure 2. Tumor specific CD8$^+$ T-cell unresponsiveness and adenocarcinoma growth are restored in Kit^{Wsh}-TRAMP mice reconstituted with BMMCs. A-D) 8 weeks old Kit^{Wsh}-TRAMP mice were reconstituted (rec) with bone marrow-derived mast cells (BMMC). Toluidine blue staining (A) on spleen and prostate sections verified reconstitution. Magnification 20x, insets 40x. At 16 weeks of age, reconstituted mice and control age-matched TRAMP, Kit^{Wsh}-TRAMP, B6 and Kit^{Wsh} mice were immunized and analyzed for *in vivo* cytotoxicity (B) and *ex vivo* IFNγ production (C) by CD8$^+$ T cells, as described in Figure 1. Experiment was repeated three times with at least 4 mice per group. Anova followed by Tukey's test: *$P <$ 0.05, **$P < 0.01$, *** $P < 0.001$. (D) Evaluation of prostatic lesions of reconstituted Kit^{Wsh}-TRAMP mice ($n = 14$) killed at 25 wk, scored by a pathologist as dysplasia/PIN, adenocarcinoma (ADENO) or neuroendocrine (NE). Control TRAMP and Kit^{Wsh}-TRAMP mice are the same cohorts reported in Fig. 1. (E-F) TRAMP and Kit^{Wsh}-TRAMP ($n = 6$ each group, pooled from two independent experiments) were depleted of T cells when 16 weeks old by surgical removal of thymus and subsequent administration of depleting anti-CD4 and anti-CD8. Treated and control untreated mice were killed at 25 weeks of age, and prostates scored by a pathologist as dysplasia/PIN, in situ ADENO or infiltrating ADENO. E) Representative H6E staining; magnification 40x. F) Evaluation of frequency of prostate lesion within each group. Fisher's test: ** $P < 0.01$, **** $P < 0.0001$.

Figure 3. Mast cells interact with PMN-MDSCs in the spleen of TRAMP mice fostering their suppressive ability. A) Representative immunofluorescence staining of spleens of 16 weeks old TRAMP mice (upper and middle panels, magnification 63x and zoomed area, respectively) and of control 16 weeks old Kit^{Wsh}-TRAMP mice

(lower panels, magnification 63x). Green: Gr1, red: Triptase, blue: CD3. B) M-MDSC-like cells ($CD11b^{+}Ly6G^{low}Ly6C^{hi}$) and PMN-MDSCs ($CD11b^{+}Ly6G^{hi}Ly6C^{int}$) FACS sorted from the spleen of TRAMP or Kit^{Wsh}-TRAMP mice (a pool of at least 4 mice/group) were tested *in vitro* for suppressive activity against T cells. Responder CFSE-labeled splenocytes were stimulated with anti-CD3 and anti-CD28 and tested after 3 days by flow cytometry. MDSC: responder ratio 1:1, 1:1.5 or 1:2 as indicated. Histogram reports percentage of proliferation for $CD4^{+}$ (left panels) or $CD4^{+}$ T cells (right panels), as indicated. Experiment was repeated three times. C) Relative expression of Arg1, iNOS, STAT3, Tgfb and IL6 as assessed by real time PCR in M-MDSC-like cells or PMN-MDSCs isolated as described above (n = 3 biological replicates or RNA of cells sorted by pools of at least 4 mice/group). Values were normalized using an internal control (GAPDH) and analyzed using the ΔΔCT method. Experiment was repeated three times. Anova followed by Tukey's test: * $P < 0.05$, ** $P < 0.01$, *** $P < 0.001$.

Figure 4. Inhibition of mast cell degranulation in TRAMP mice has no effect on tumor specific T-cell activity and only partially inhibits adenocarcinoma growth. TRAMP and wild type C57BL6 (B6) mice were treated daily with Cromolyn, from 8 weeks of age. A-B) At 16 weeks of age, treated mice and control age-matched untreated TRAMP and B6 mice were immunized and analyzed for *in vivo* cytotoxicity (A) and *ex vivo* IFNγ production (B) by Tag-specific $CD8^{+}$ T cells as described in figure 1. Experiment was repeated two times with 5 mice per group. Anova followed by Tukey's test: * $P < 0.05$, ** $P < 0.01$, *** $P < 0.001$. C) Alternatively, TRAMP mice were treated with Cromolyn until 25 weeks of age, and prostates collected for histopathology (n = 12). Histogram depicts the relative percentage of dysplasia/PIN,

adenocarcinoma (ADENO) or neuroendocrine (NE) lesions as scored by a pathologist. Control TRAMP and Kit^{Wsh}-TRAMP mice are the same cohorts reported in Fig. 1. Fisher's Test: **** $P < 0.0001$.

Figure 5. Mast cells interact with PMN-MDSCs via CD40L-CD40 increasing their suppressive activity. A) Representative immunofluorescence staining of spleens of 16 weeks old TRAMP mice. Green: CD40, red: Triptase, blue: Gr1. B) 8 weeks old Kit^{Wsh}-TRAMP mice were reconstituted (rec) with bone marrow-derived mast cells isolated from wild-type (BMMC) or CD40L$^{-/-}$ (BMMC CD40L$^{-/-}$) mice. At 16 weeks of age, PMN-MDSCs were FACS sorted from the spleen of reconstituted mice and of control age-matched TRAMP and Kit^{Wsh}-TRAMP mice (a pool of at least 4 mice/group), and were tested *in vitro* for suppressive activity against T cells, as described in Fig. 3. Histogram reports percentage of proliferation for CD4$^+$ (left panel) or CD8$^+$ T cells (right panel). Experiment was repeated three times. C) Relative expression of Arg1, iNOS and STAT3, as assessed by real time PCR, in PMN-MDSCs isolated as described above ($n = 2$ biological replicates or RNA of cells sorted by pools of at least 4 mice/group). Values were normalized using an internal control (GAPDH) and analyzed using the ΔΔCT method. Experiment was repeated three times. D) PMN-MDSCs, FACS-sorted from the spleen of Kit^{Wsh}-TRAMP mice were seeded either alone, or in the presence of BMMC (ratio 1:1) from wild type (MC) or CD40L$^{-/-}$ (MC CD40L$^{-/-}$), or with 10μg/of agonistic anti-CD40 or antagonistic anti-CD40L. Two biological replicates/group. As positive control cells were stimulated with IL4 and IFNγ. The following day cells were stained with surface anti-CD11b and anti-cKit, and with probes detecting intracellular RNA transcripts for Arg1, iNOS and Stat3, according to the PrimeFlow RNA assay protocol. Flow

cytometry plots explain the gating strategy and histogram report relative fluorescence intensity, measured as ratio of mean fluorescence intensity between the sample and a control sample not stained with the indicated probe. Experiment was repeated three times. Anova followed by Tukey's test: * $P < 0.05$, ** $P < 0.01$, *** $P < 0.001$, **** $P < 0.0001$.

Figure 6. Tumor-specific CD8$^+$ T-cell unresponsiveness and adenocarcinoma growth are not restored in Kit^{Wsh}-TRAMP mice reconstituted with CD40L$^{-/-}$ BMMCs. A-B) 8 weeks old Kit^{Wsh}-TRAMP mice were reconstituted with bone marrow-derived mast cells, either from wild-type (BMMC) or CD40L$^{-/-}$ (BMMC CD40L$^{-/-}$) mice. At 16 weeks of age, reconstituted (rec) mice and control age-matched TRAMP, Kit^{Wsh}-TRAMP and C57BL6 (B6) mice were immunized and analyzed for *in vivo* cytotoxicity (A) and *ex vivo* IFNγ production (B) by CD8$^+$ T cells as described in figure 1. Experiment was repeated three times with at least 4 mice per group. Anova followed by Tukey's test: *$P < 0.05$, **$P < 0.01$, *** $P < 0.001$. C) Alternatively, mice ($n = 4$ for each group) were killed at 25 weeks of age. Prostates were evaluated by a pathologist, for quantitation of areas of dysplasia/PIN (contoured in blue), in situ adenocarcinoma (contoured in red) or infiltrating adenocarcinoma (contoured in black). Magnification 50x. D) Graph depicts the relative percentage of each lesion on total tumor burden for each mouse. Experiment was repeated twice. Fisher's Test: ** $P < 0.01$, *** $P < 0.001$, **** $P < 0.0001$.

Figure 7. High expression of mast cell and PMN-MDSC genes is associated with poor clinical outcome of prostate cancer patients. A) A high expression of 20 genes, peculiar to mast cells and PMN-MDSCs, is associated to an increased

biochemical relapse-free survival. Kaplan-Meier curve is represented. Prostate cancer patients were stratified in 2 groups depending on a high (above the median) or low (below the median) mean expression of the 20 mast cell/PMN-MDSC–associated genes found in the Chiorino dataset. The number of events is reported in brackets for the two groups. B) 19/20 genes are able to predict recurrence-free survival on the independent Taylor dataset of 140 prostate cancer patients in a statistically significant manner. Patients were stratified as in A. C) 13/20 genes present in the Setlur dataset were predictive for overall survival of the 358 prostate cancer patients of this data set. Patients were stratified as in A. D) Venn diagram showing the overlap between gene signatures among the three different datasets (left panel). Partial overlaps are due to different platforms used for microarray experiments. The list of genes tested for each dataset is reported on the right side of the panel.

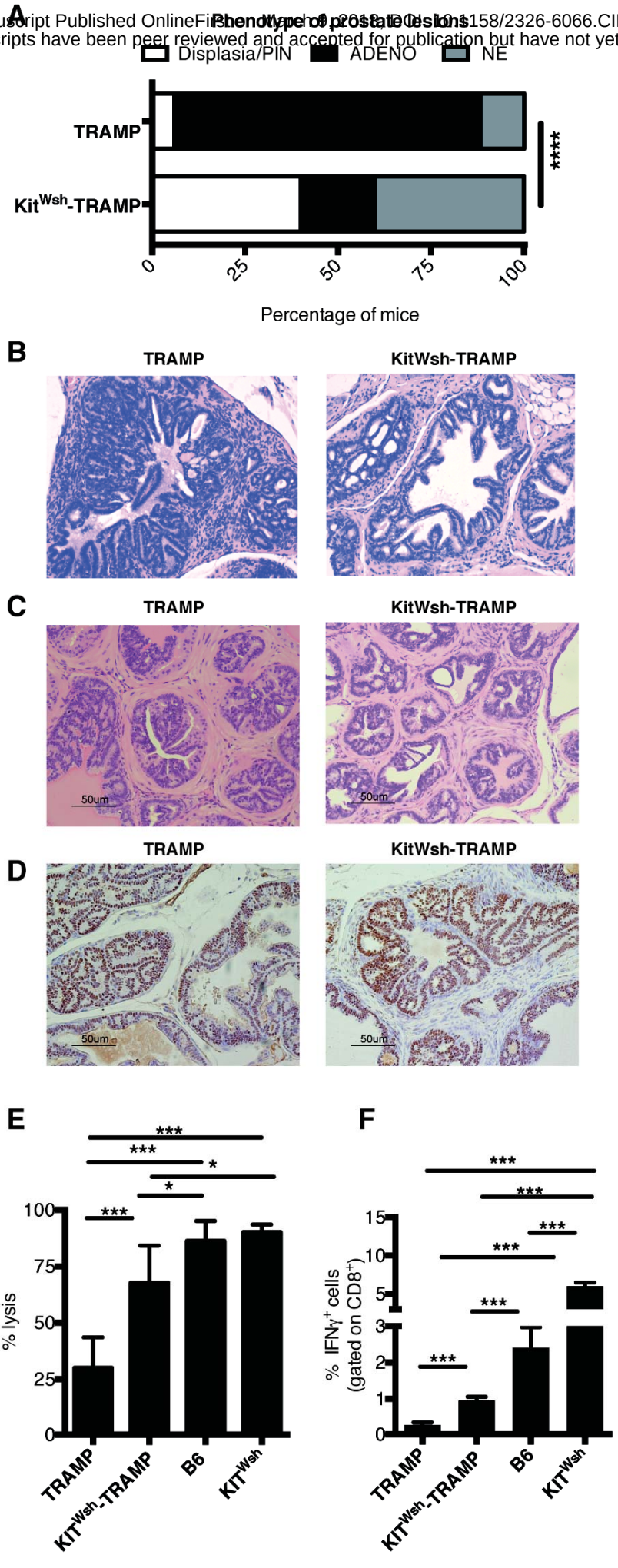

Jachetti, MC MDSC, Fig.1

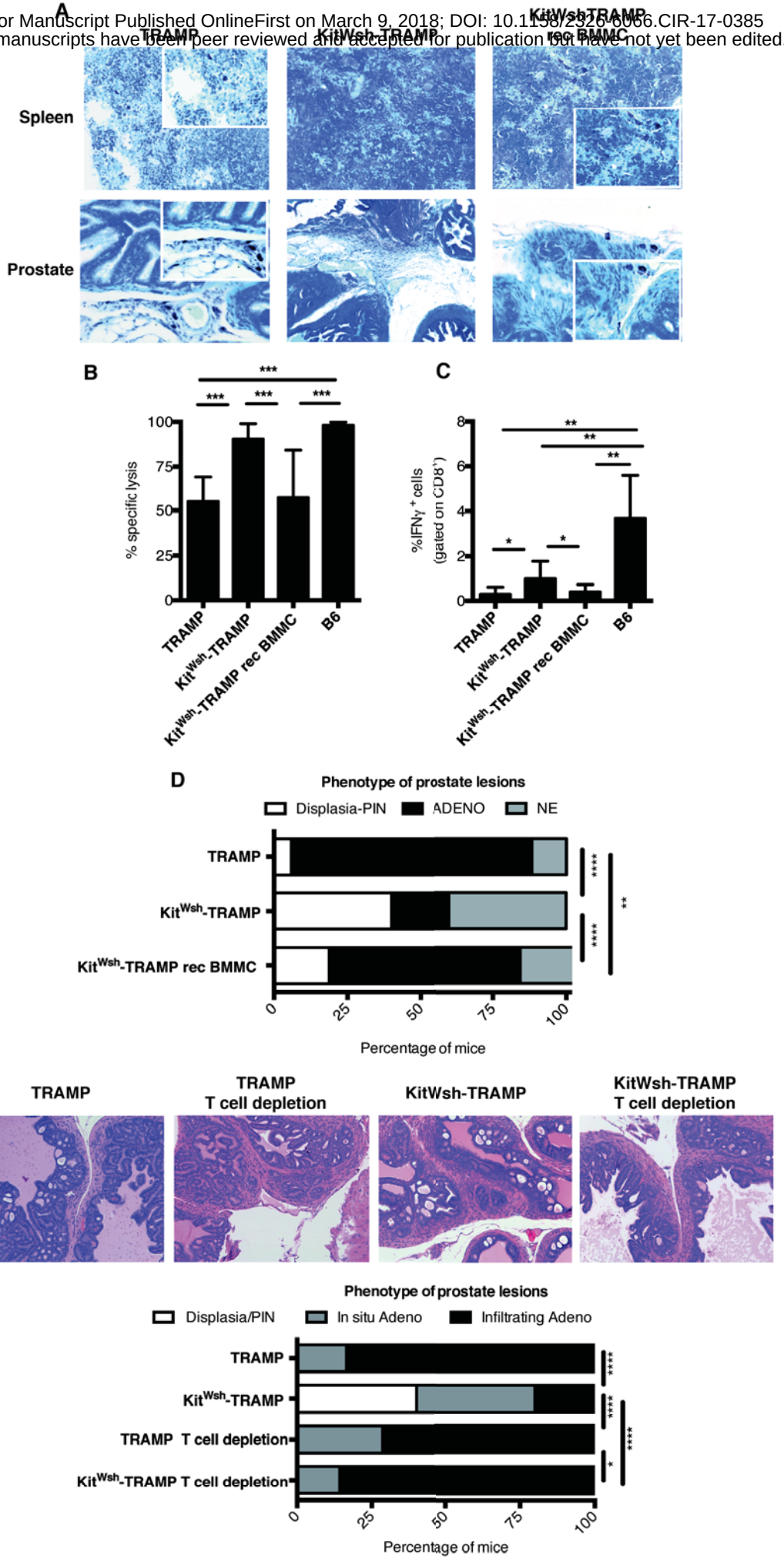

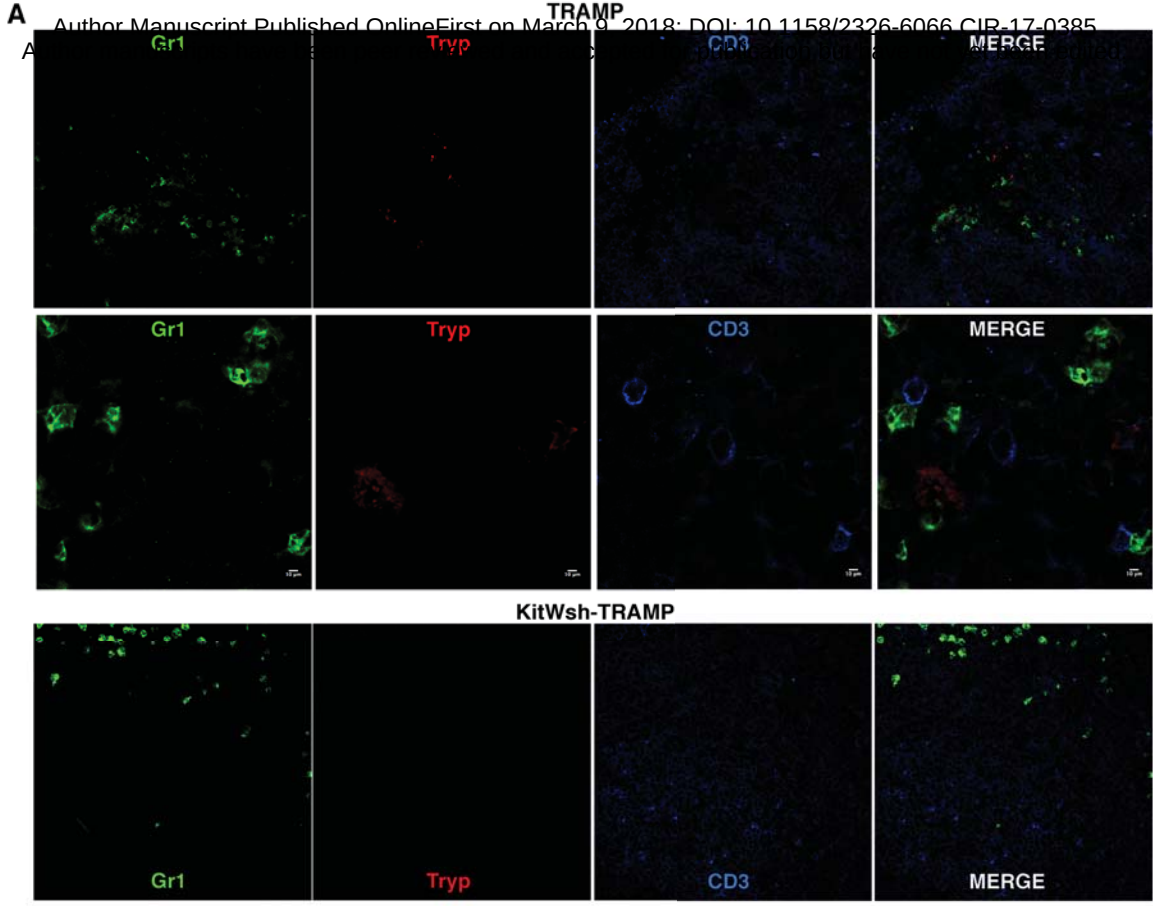

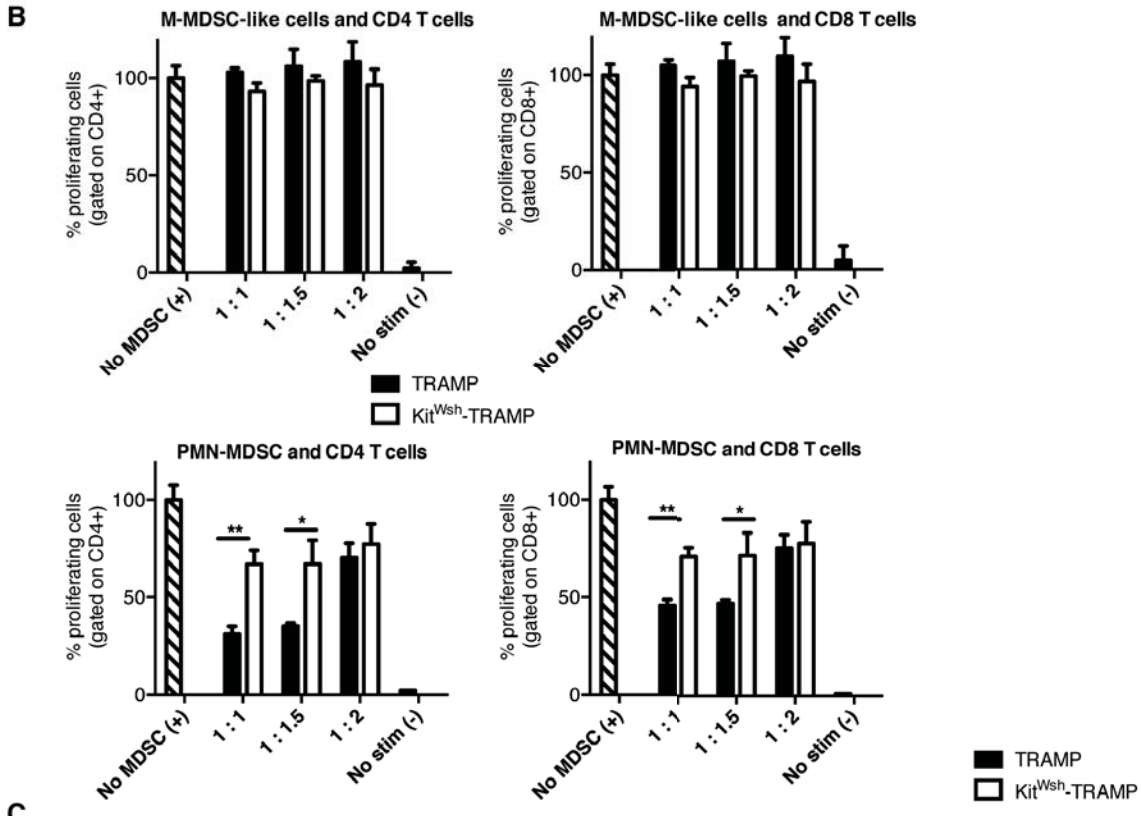

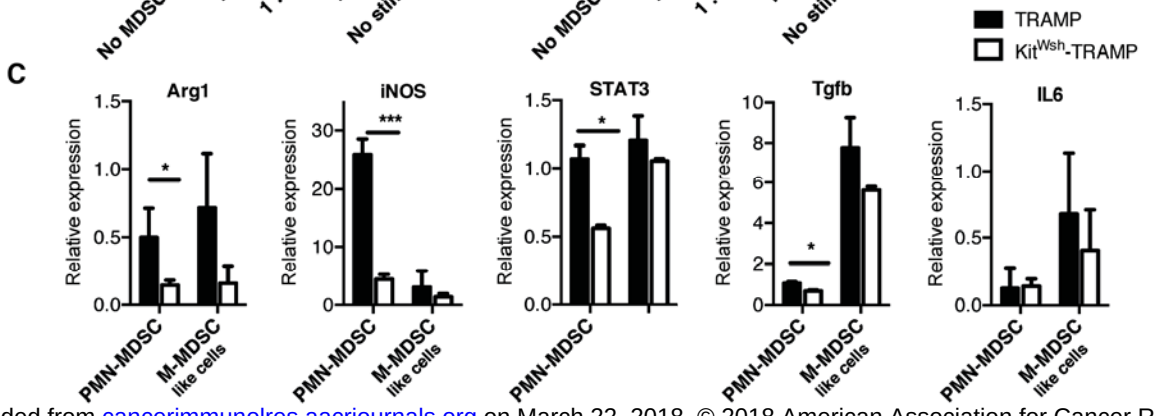

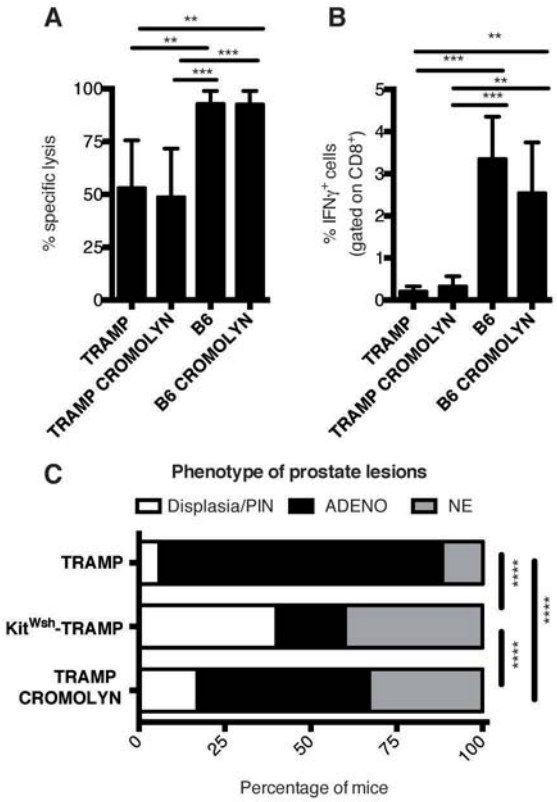

Jachetti MC MDSC, Fig. 4

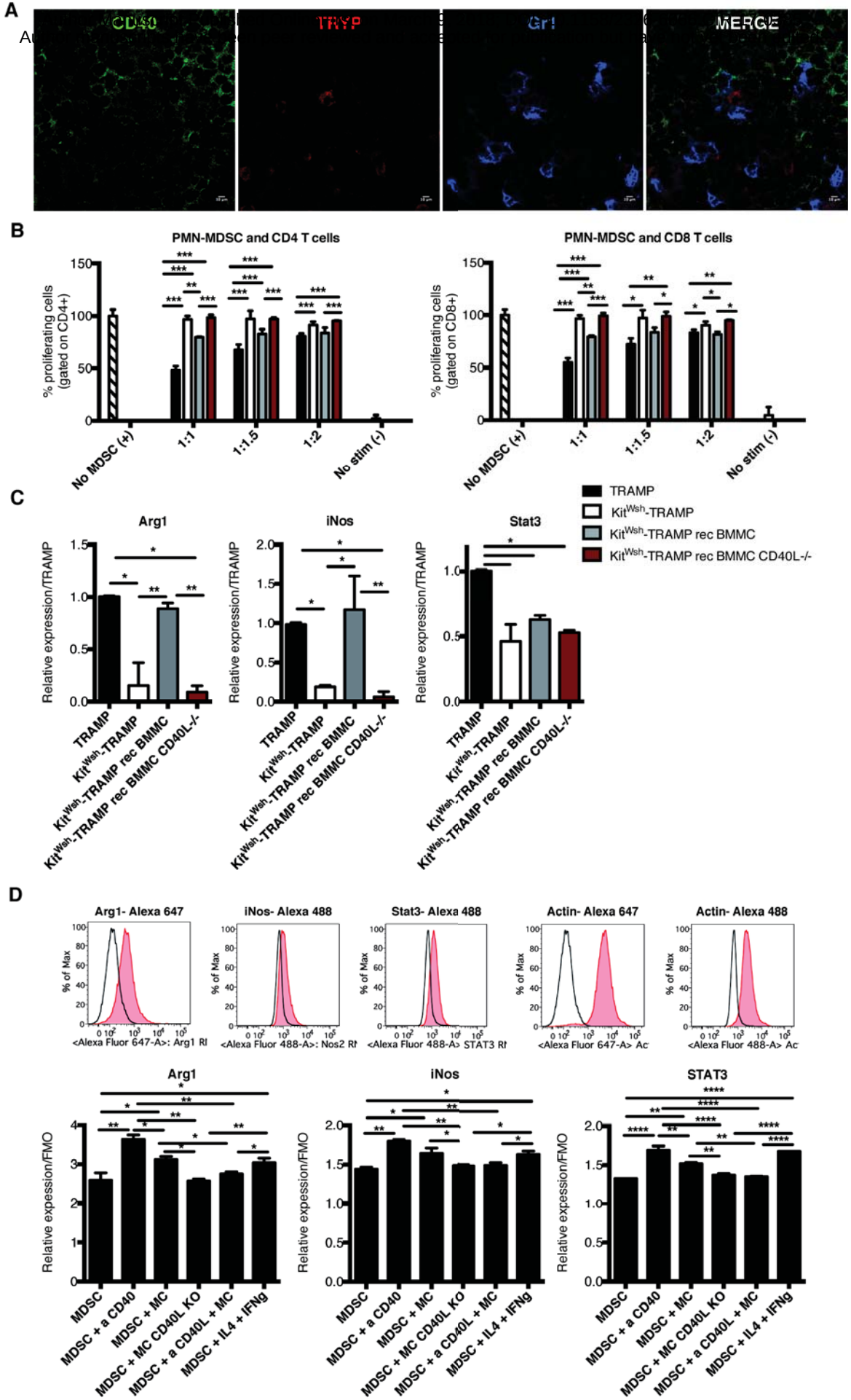

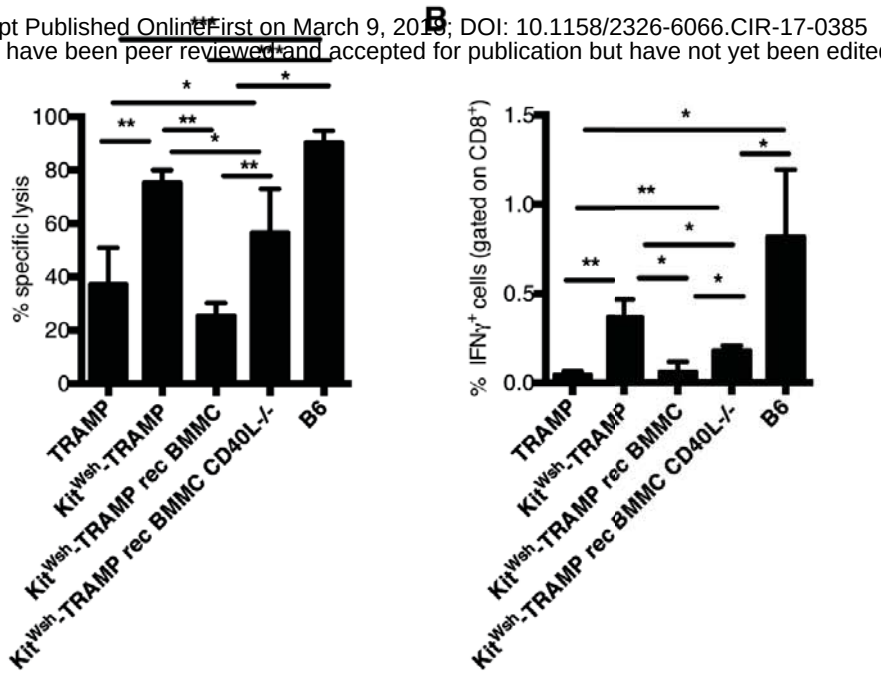

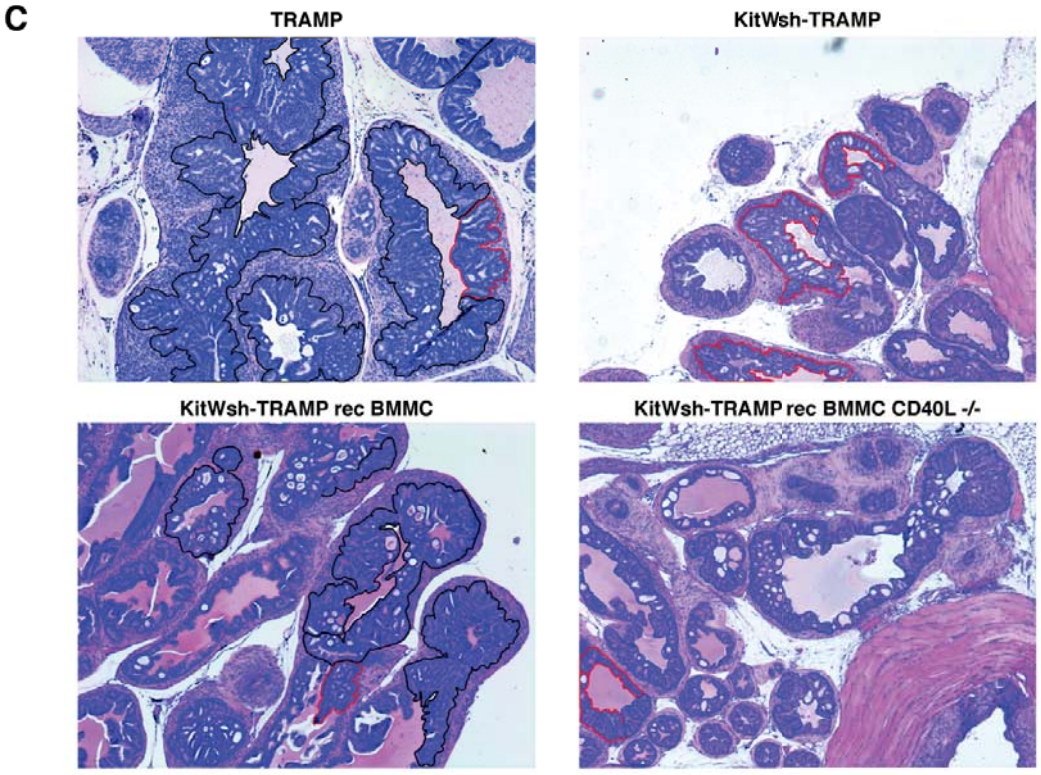

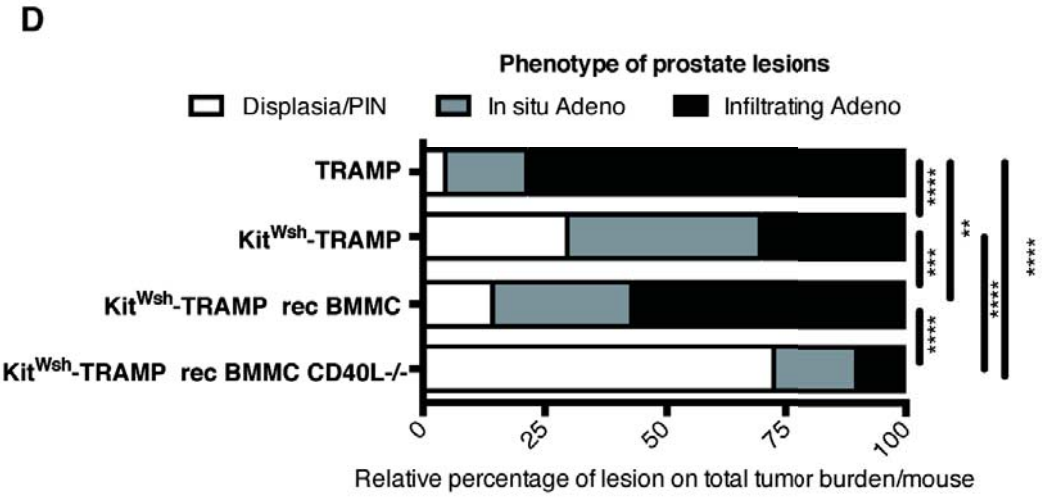

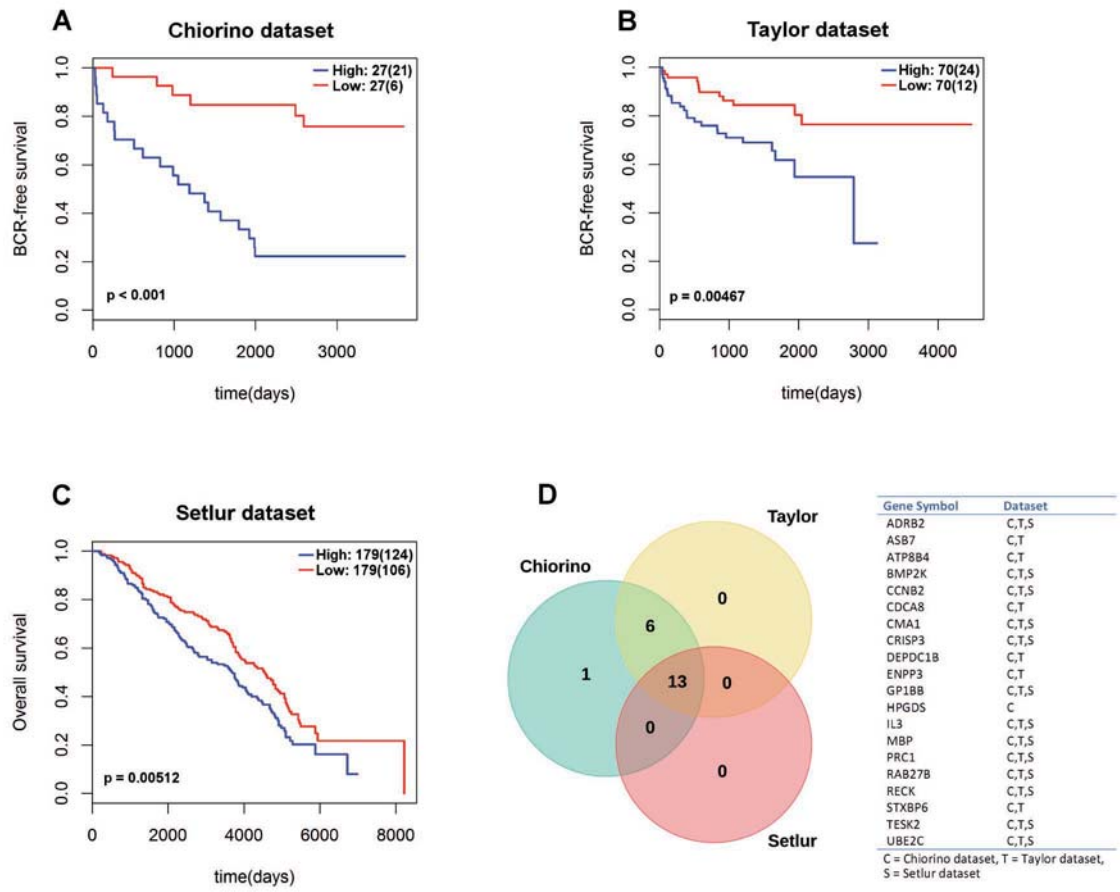

Gene Symbol	Dataset
ADRB2	C,T,S
ASB7	C,T
ATP8B4	C,T
BMP2K	C,T,S
CCNB2	C,T,S
CDCA8	C,T
CMA1	C,T,S
CRISP3	C,T,S
DEPDC1B	C,T
ENPP3	C,T
GP1BB	C,T,S
HPGDS	C
IL3	C,T,S
MBP	C,T,S
PRC1	C,T,S
RAB27B	C,T,S
RECK	C,T,S
STXBP6	C,T
TESK2	C,T,S
UBE2C	C,T,S

C = Chiorino dataset, T = Taylor dataset, S = Setlur dataset

Jachetti, MC MDSC, Fig.7

Jachetti et al, MC MDSC, Supplementary Data

Including 10 supplementary figures

SUPPLEMENTARY FIGURES

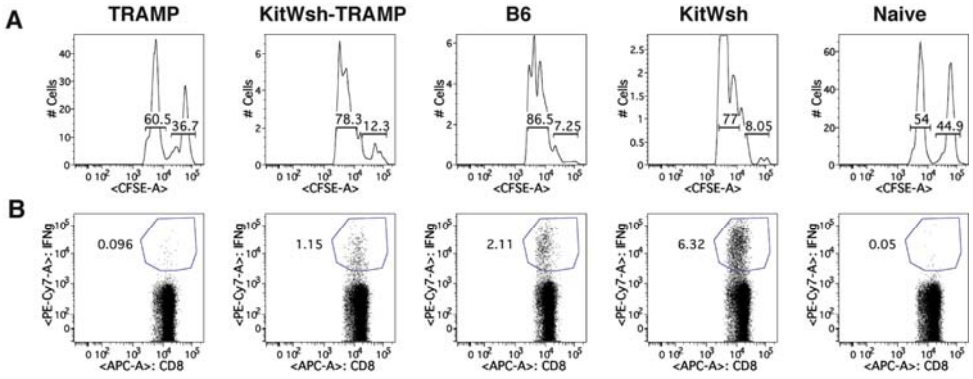

Jachetti, MC MDSC, Suppl. Fig.1

Supplementary Figure 1. Representative plots illustrating analysis of tumor-specific CD8$^+$ T cell response in TRAMP and Kit^{Wsh}-TRAMP mice. 16 weeks old TRAMP, Kit^{Wsh}-TRAMP or control C57BL6 or Kit^{Wsh} mice were immunized with DC pulsed with TagIV peptide. Seven days later Tag specific *in vivo* cytotoxicity and *ex-vivo* IFNγ production by CD8 T cells were tested as described in Figure 1. A) Representative histograms showing peaks of CFSE^{High} and CFSE^{low} injected cells, gated on 7AAD negative cells. B) Representative dot plots showing IFNg$^+$CD8$^+$ cells. Plots are gated within CD8$^+$ T cells.

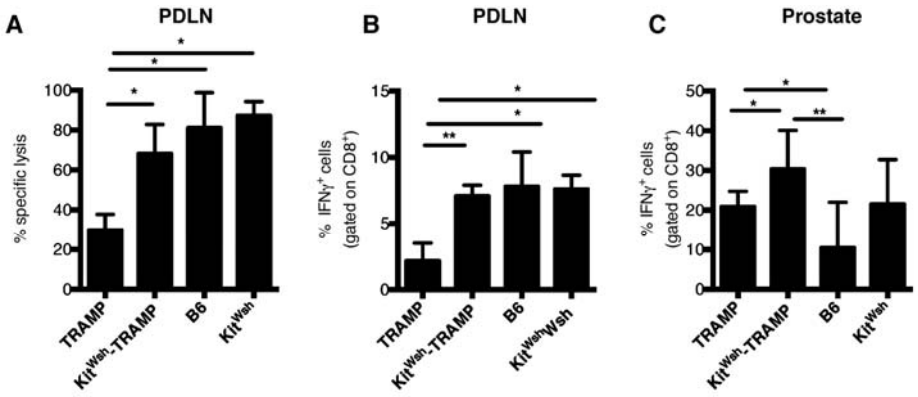

Jachetti, MC MDSC, Suppl. Fig. 2

Supplementary Figure 2. CD8$^+$T cells from PDLN and prostates of Kit^{Wsh}-TRAMP mice are responsive. 16 weeks old TRAMP, Kit^{Wsh}-TRAMP or control C57BL6 or Kit^{Wsh} mice were treated as described in Figure 1. **A)** Quantification of Tag specific lysis from cells isolated from PDLN **(B-C)** Quantification of IFNγ production by PMA-Ionomycin stimulated CD8$^+$ T cells, isolated from PDLN (B) or prostates (C). Values are subtracted of background, i.e. spontaneous IFNγ release by unstimulated CD8$^+$ T cells. Experiments were repeated three times with at least 4 mice per group. Anova followed by Tukey's test: *$p<0.05$, **$p<0.01$.

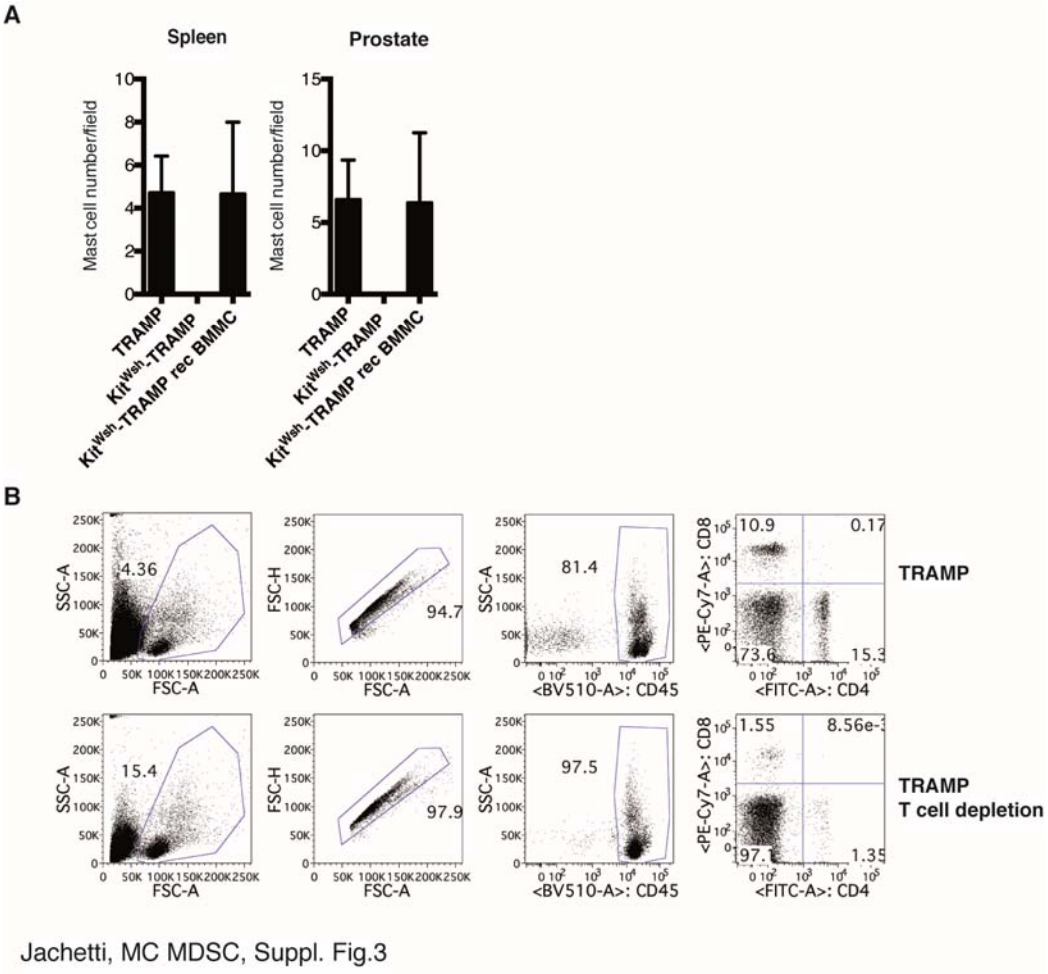

Supplementary Figure 3. Quantification of MCs or T cells after reconstitution of depletion, respectively. A) 8 weeks old Kit^{Wsh}-TRAMP mice were reconstituted (rec) with bone marrow-derived MCs (BMMC) and killed 8 weeks later as reported in Figure 2. Quantification of MCs infiltrating spleen and prostates of TRAMP, Kit^{Wsh}-TRAMP and reconstituted (rec) Kit^{Wsh}-TRAMP mice was performed on toluidine blue stained sections. MCs counts reported are an average of the count preformed in 5 fields per section. B) T cell depletion in 16 weeks old TRAMP and Kit^{Wsh}TRAMP was obtained by surgical removal of thymus and subsequent administration of depleting anti CD4 and anti CD8 antibodies. Effective T cell depletion was checked by flow cytometry, representative dot plots are shown.

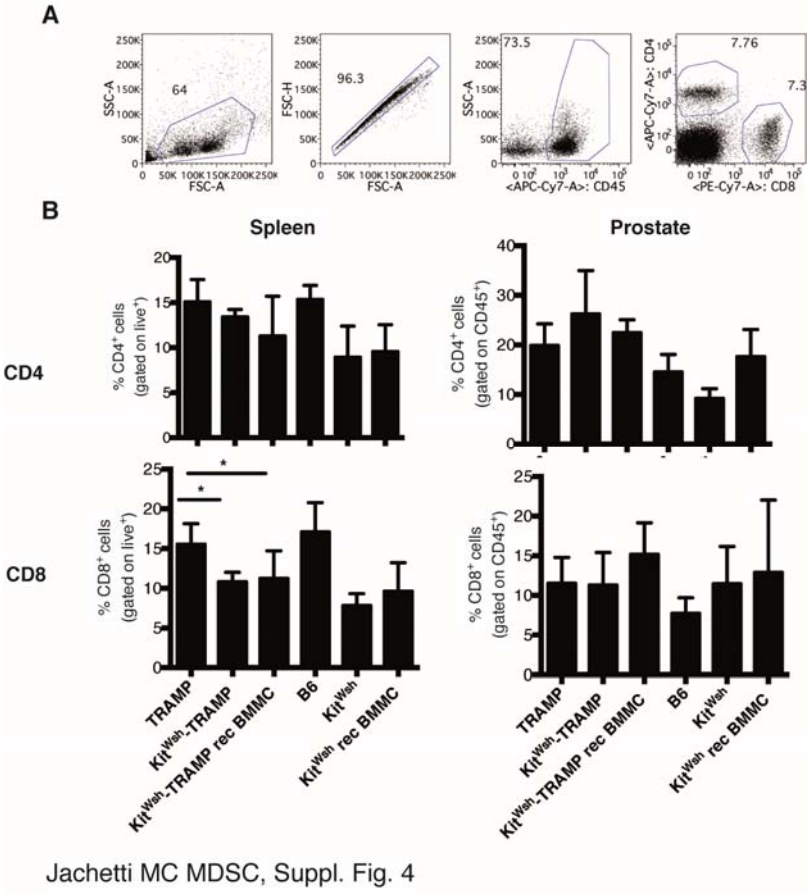

Supplementary Figure 4. Flow cytometry identification of T cells in spleen and prostate of TRAMP and Kit^{Wsh}-TRAMP mice. A) Representative dot plots indicating the gating strategy adopted analyzing cell obtained from spleen or prostates of mice. CD4$^+$ and CD8$^+$ T cells were gated on live cells or on CD45$^+$ cells in spleens. B) Histogram reports the percentages of CD4$^+$ and CD8$^+$ T cells within spleen and prostate of the indicated groups of mice. Experiment was repeated three times with at least 4 mice per group. Anova followed by Tukey's test: *p<0.05, **p<0.01, *** p<0.001.

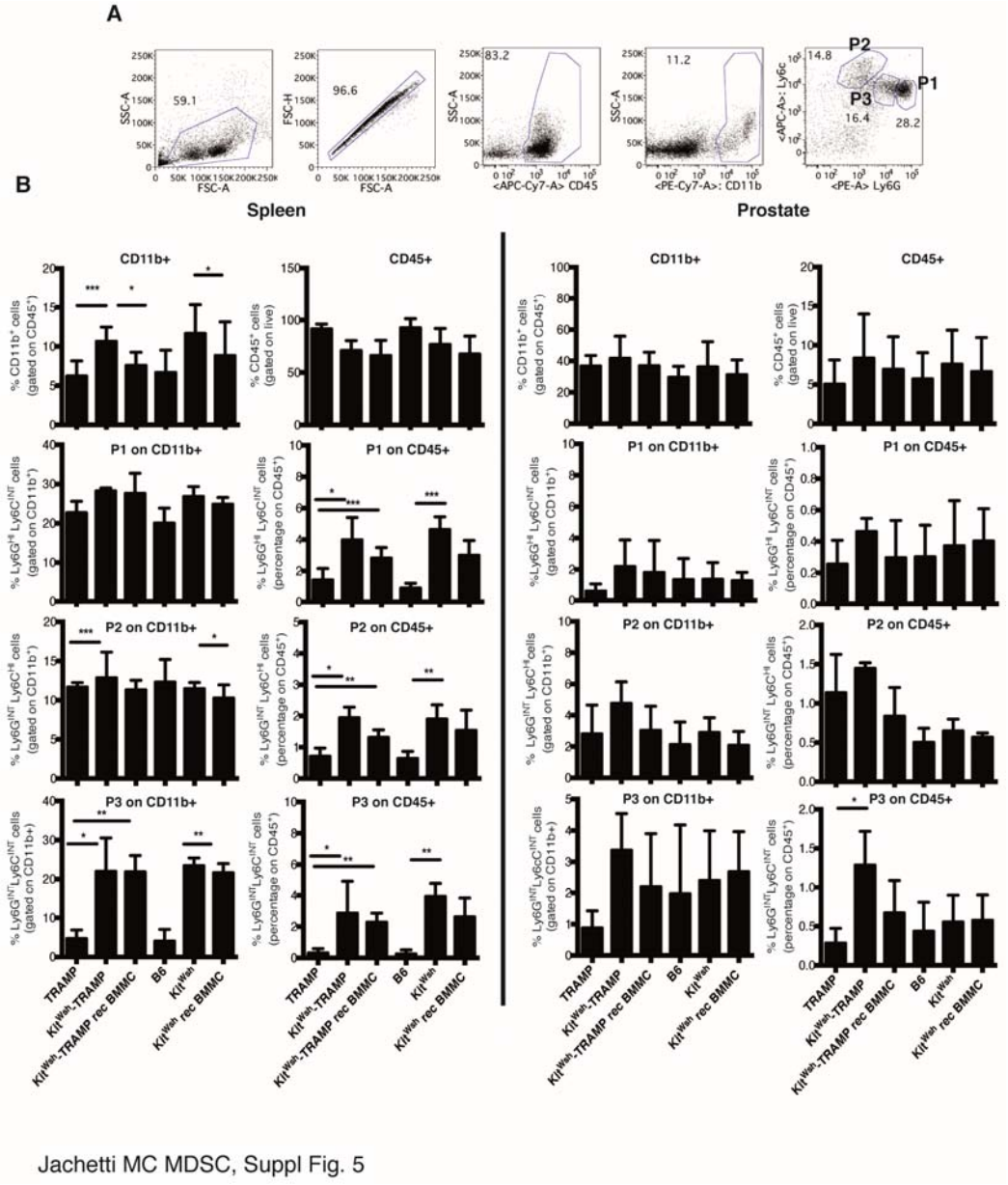

Supplementary Figure 5. Flow cytometry identification of myeloid cells in spleen and prostate of TRAMP and Kit^{Wsh}-TRAMP mice. A) Representative dot plots indicating the gating strategy adopted analyzing cell obtained from spleen or prostates of mice. CD11b^{+} cells were gated on CD45^{+} cells in both organs. Ly6G and Ly6C were used to identify PMN-MDSC (Ly6G^{HI}Ly6C^{LOW}; P1), M-MDSC like-cells (Ly6G^{Low}Ly6C^{HI}; P2) or immature granulocytic precursors (Ly6G^{INT}Ly6C^{INT}; P3) among CD11b^{+} cells. B) Histogram reports the percentages of the above cited

myeloid cell populations within spleen and prostate of the indicated groups of mice. Cells are gated on $CD11b^+$ or $CD45^+$ as indicated. Experiment was repeated three times with at least 4 mice per group. Anova followed by Tukey's test: *p<0.05, **p<0.01, *** p<0.001.

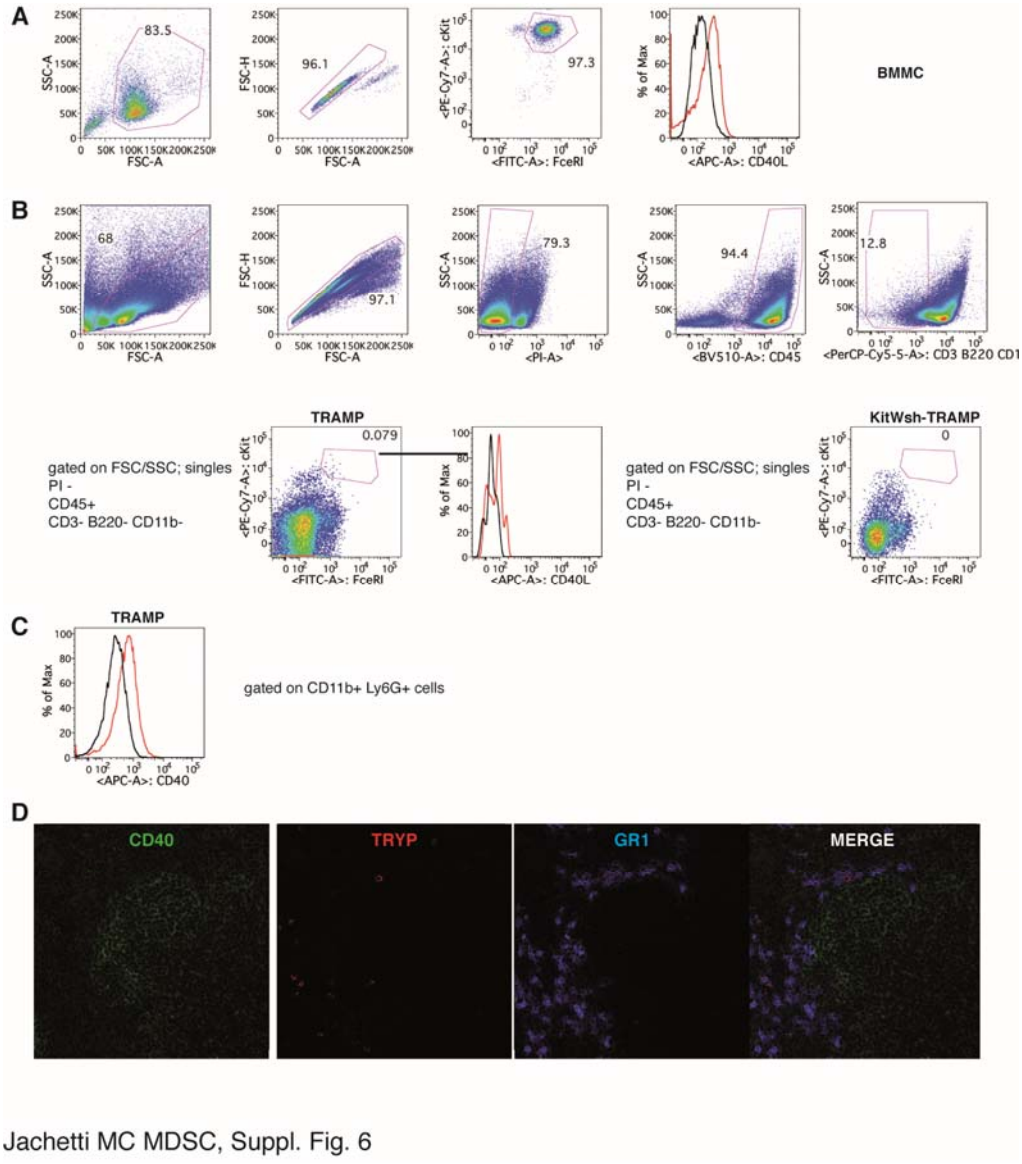

Supplementary Figure 6. MCs and PMN-MDSC can interact via CD40L-CD40 in TRAMP mice. A) Representative gating strategy (FSC/SSC, Singles, $cKit^+FceRI^+$) and CD40L staining on *in vitro* cultured BMMC derived from wild type (red

histogram) or CD40L$^{-/-}$ mice (black histogram). B) Representative dot plot illustrating the gating strategy for identification of cKit^{+}FceRI^{+} MCs in the spleen of 16 weeks old TRAMP mice (FSC/SSC, Singles, PI^{-}, CD45^{+}, CD3^{-} B220^{-} CD11b^{-}). Histogram report CD40L expression on gated cells (red histogram: specific staining; black histogram: isotype control). With the same gating strategy, no cKit^{+}FceRI^{+} cells were found in the spleen of Kit^{Wsh}-TRAMP mice, analyzed as negative control. C) Splenocytes from 16 weeks old TRAMP mice were analyzed by flow cytometry. Histogram report CD40 staining on CD11b^{+}Ly6G^{+} gated cells (red histogram: specific staining; black histogram: isotype control). D) Representative immunofluorescence staining on the follicular B cell zone of the spleen of 16 weeks old TRAMP mice. Green: CD40, red: Triptase, blue: Gr1. Magnification 63x.

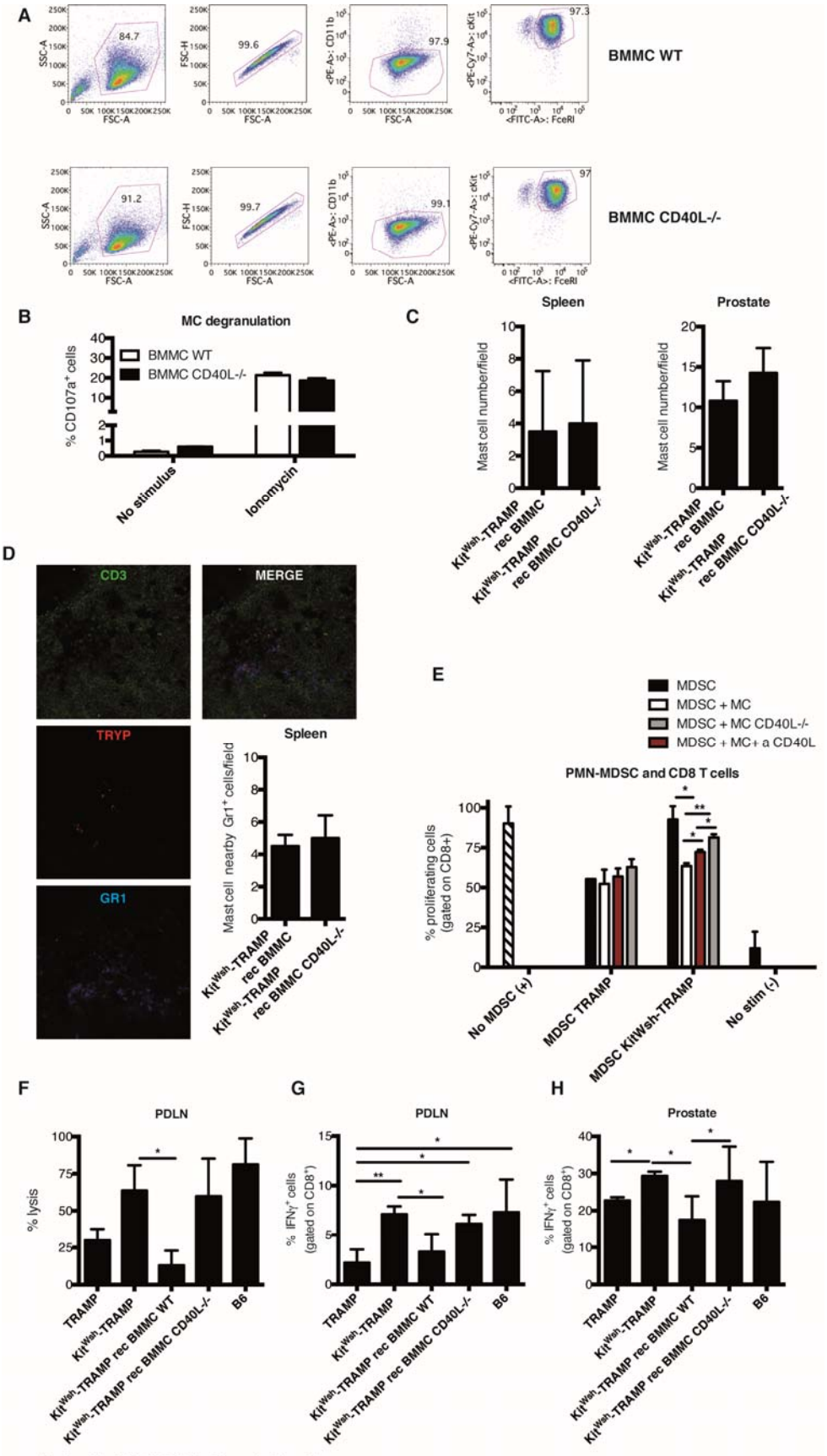

Jachetti, MC MDSC, Suppl. Fig. 7

Supplementary Figure 7. Wild type and CD40L$^{-/-}$ BMMC are equally functional, but CD8^{+}T cells from PDLN and prostates of Kit^{Wsh}-TRAMP mice reconstituted with BMMC CD40L$^{-/-}$ are still responsive. A) Bone marrow precursors from congenic C57BL6/J or CD40L$^{-/-}$ mice were cultured in vitro in RPMI with 20% FBS, and 20 ng/ml of both SCF and IL-3 (Peprotech) (10). After 4 weeks, purity was evaluated by flow cytometry (CD11b-, FcεRI+ cKit+ cells). B) Wild type and CD40L$^{-/-}$ BMMC were left untreated or stimulated with Ionomycin (1μg/ml) for 30'. Degranulation was tested as membrane CD107a expression by flow cytometry.

C) Quantification of MCs infiltrating spleen and prostates of Kit^{Wsh}-TRAMP reconstituted (rec) with BMMC WT or CD40L$^{-/-}$ was performed on toluidine blue stained sections. Histograms report MCs counts as average of the count preformed in 5 fields per section. D) Representative immunofluorescence staining of spleen of mice described in (C), showing proximity of MCs with Gr1^{+} cells in reconstituted Kit^{Wsh}-TRAMP mice. Green: CD3, red: Triptase, blue: Gr1 Magnification 63X. Histograms reports count of MCs in proximity of Gr1^{+} cells, as an average of 3 fields per section (n=3 mice/group). E) PMN-MDSC were FACS sorted from the spleen of TRAMP and Kit^{Wsh}-TRAMP mice (a pool of at least 4 mice/group), and tested *in vitro* for suppressive activity against T cells, as described in figure 3 (responder:MDSC ratio = 1:1). Where indicated wild type or CD40L$^{-/-}$ MCs (Ratio 1:1) or anti CD40L blocking antibody (10 μg/ml) were added. F-H) 16 weeks old Kit^{Wsh}-TRAMP previously reconstituted (rec) with wild type or CD40L$^{-/-}$ BMMC, or age-matched TRAMP, Kit^{Wsh}-TRAMP or control B6 mice were treated as described in Figure 6. Histograms report quantification of Tag specific lysis from cells isolated from PDLN (F) and quantification of IFNγ production by PMA-Ionomycin stimulated CD8^{+} T cells,

isolated from PDLN (F) or prostates (G). Values are subtracted of background, i.e. spontaneous IFNγ release by unstimulated $CD8^+$ T cells. Experiments were repeated three times with at least 4 mice per group. Anova followed by Tukey's test: *$p<0.05$.

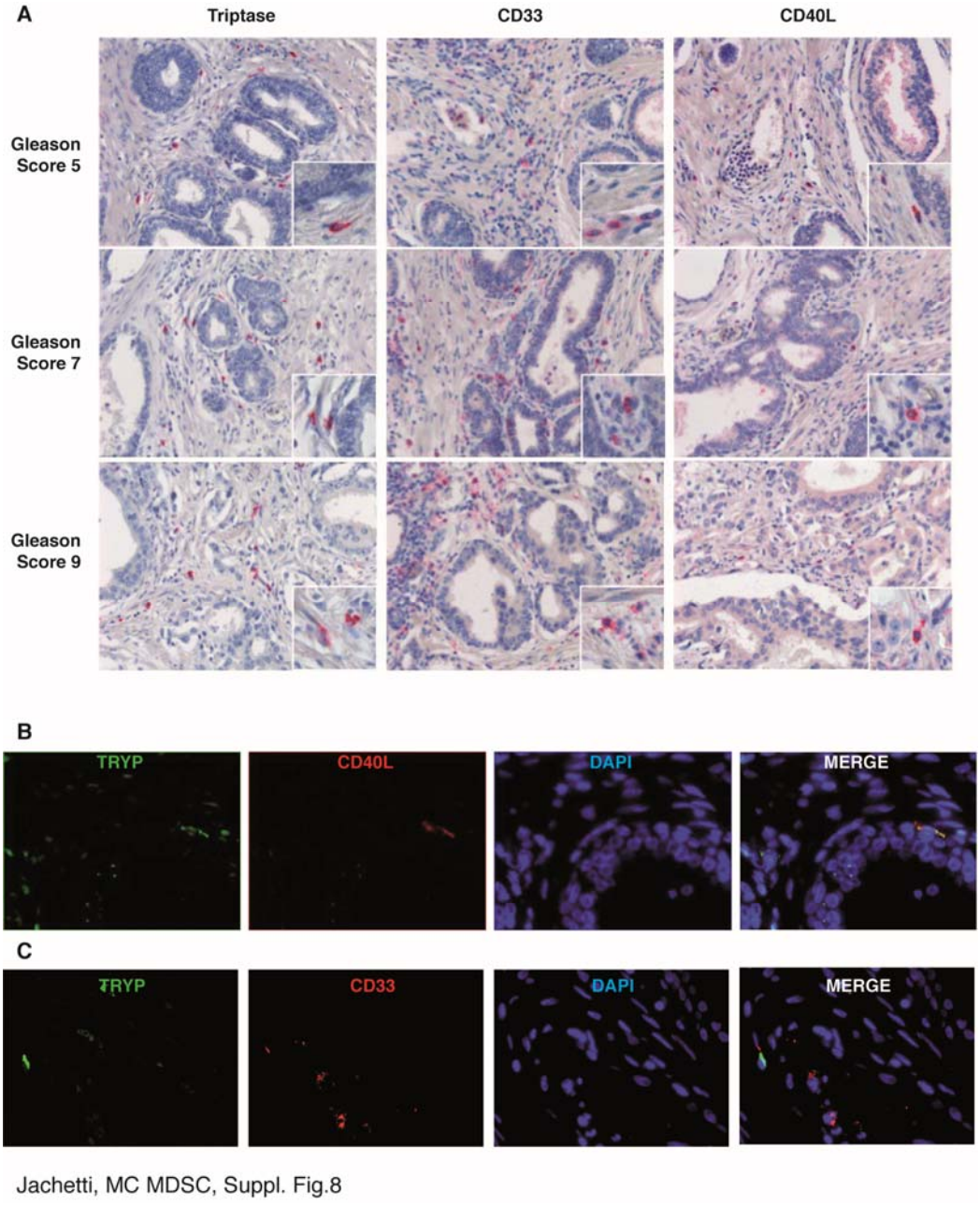

Jachetti, MC MDSC, Suppl. Fig.8

Supplementary Figure 8. MCs, CD40L and CD33 co-localize in human tumor prostate cancer samples. A) Immunohistochemistry for Triptase, CD40L or CD33 on serial section of human prostate cancer samples representative of different stages (Gleason Score 5, 7 or 9). Magnification 20X, insets 40x. B) Representative immunofluorescence staining on the same human prostate cancer samples. Green: Tryptase, red: CD40L, blue: DAPI. Magnification 63X. C) Representative immunofluorescence staining on the same same human prostate cancer samples. Green: Tryptase, red: CD33, blue: DAPI. Magnification 63X.

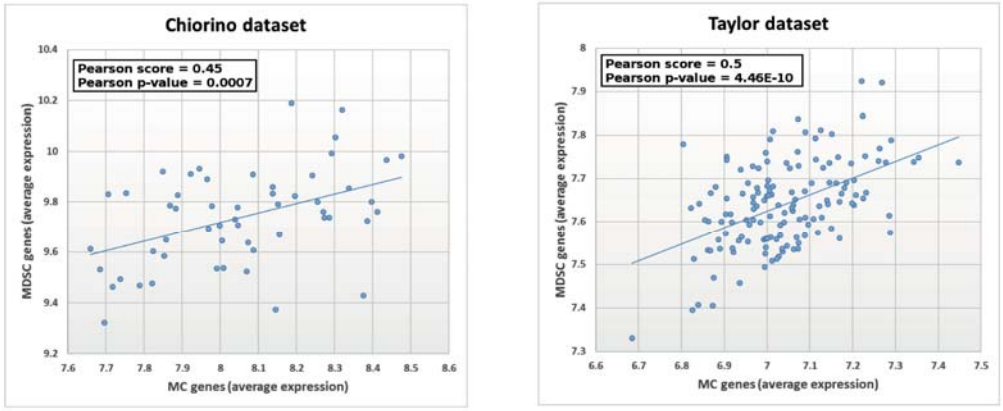

Jachetti, MC MDSC, Suppl. Fig.9

Supplementary Figure 9. Correlation between MC-genes and MDSC-activity genes in human prostate cancer data sets. We created two metagenes for the Chiorino's and Taylor's datasets. Each metagene is an aggregate pattern of gene expression, in this case given by the average, for MC and MDSC-suppressive genes respectively, obtained by genes in Supplementary Table 1. We then calculated Pearson correlation between the two metagenes, demonstrating a statistically significant positive correlation in both prostate cancer datasets (Chiorino's dataset:

Pearson score = 0.45 and Pearson p-value = 0.0007; Taylor's dataset: Pearson score = 0.5 and Pearson p-value = 4.46E-10).

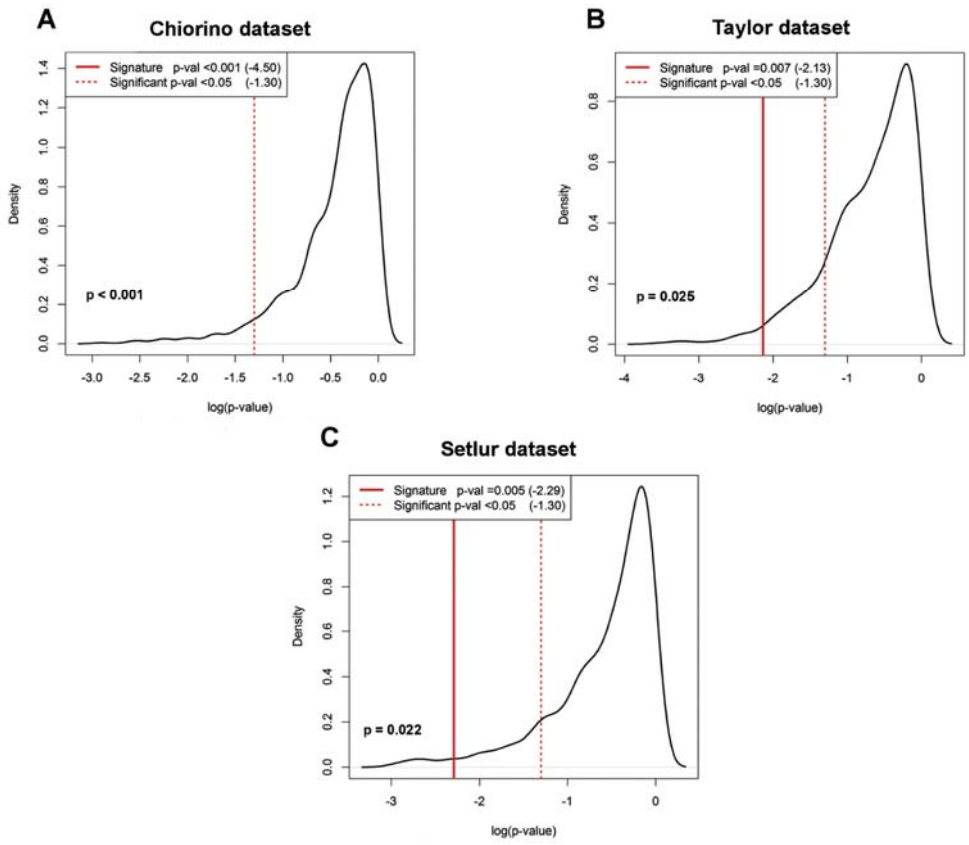

Jachetti, MC MDSC, Suppl. Fig.10

Supplementary Figure 10. MC/PMN-MDSC signatures outperform random signatures of the same length. Signatures performance on BCR-free (Chiorino's dataset, A and Taylor's dataset, B) or overall survival (Setlur's dataset, C) was tested on 1000 random gene signatures of the same length, separately for each dataset. X-axis represents survival p-values on a log 10 scale. Y-axis represents the density distribution of log10 p-values for the 1000 random signatures. The solid red vertical line corresponds to the performance of the signature being tested. The further to the left this line is, the more uniquely it performs for this check. In A, the line is not

drawn since the signature is out of the range of the background distribution. The vertical red dotted line corresponds to p=0.05.